Article

Structure

Structure of Yeast OSBP-Related Protein Osh1 Reveals Key Determinants for Lipid Transport and Protein Targeting at the Nucleus-Vacuole Junction

Graphical Abstract

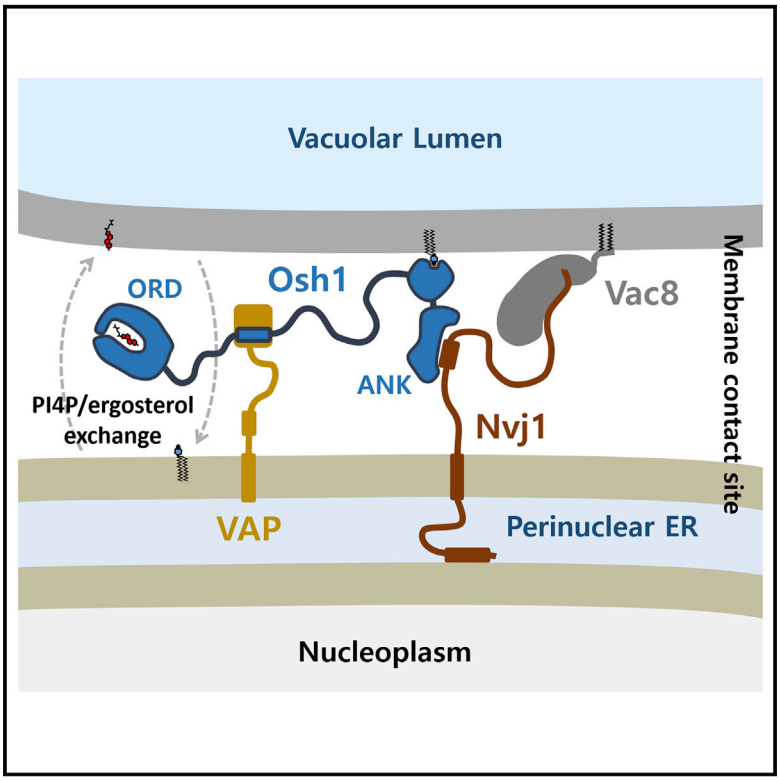

Authors

Mohammad Kawsar Manik, Huiseon Yang, Junsen Tong, Young Jun Im

Correspondence

imyoungjun@jnu.ac.kr

In Brief

The structure of Osh1 ANK and ORD domains with their cognate ligands reveals the basis for sterol/PI(4)P counter-transport and protein targeting at the nucleus-vacuole junction.

Highlights

- Osh1 ANK domain displaying a bi-lobed structure binds a cytosolic segment of Nvj1
- Nvj1 binding contributes to localization of Osh1 to the nucleus-vacuole junctions
- Osh1 ORD has a conserved β-barrel fold and binds ergosterol and PI(4)P
- Osh1 may counter-transport ergosterol and PI(4)P at the nucleus-vacuole junctions

Manik et al., 2017, Structure *25*, 617–629
April 4, 2017
http://dx.doi.org/10.1016/j.str.2017.02.010

Structure
Article

Structure of Yeast OSBP-Related Protein Osh1 Reveals Key Determinants for Lipid Transport and Protein Targeting at the Nucleus-Vacuole Junction

Mohammad Kawsar Manik,[1,2] Huiseon Yang,[1,2] Junsen Tong,[1,2] and Young Jun Im[1,3,*]
[1]College of Pharmacy, Chonnam National University, Gwangju 61186, Republic of Korea
[2]Co-first author
[3]Lead Contact
*Correspondence: imyoungjun@jnu.ac.kr
http://dx.doi.org/10.1016/j.str.2017.02.010

SUMMARY

Yeast Osh1 belongs to the oxysterol-binding protein (OSBP) family of proteins and contains multiple targeting modules optimized for lipid transport at the nucleus-vacuole junction (NVJ). The key determinants for NVJ targeting and the role of Osh1 at NVJs have remained elusive because of unknown lipid specificities. In this study, we determined the structures of the ankyrin repeat domain (ANK), and OSBP-related domain (ORD) of Osh1, in complex with Nvj1 and ergosterol, respectively. The Osh1 ANK forms a unique bi-lobed structure that recognizes a cytosolic helical segment of Nvj1. We discovered that Osh1 ORD binds ergosterol and phosphatidylinositol 4-phosphate PI(4)P in a competitive manner, suggesting counter-transport function of the two lipids. Ergosterol is bound to the hydrophobic pocket in a head-down orientation, and the structure of the PI(4)P-binding site in Osh1 is well conserved. Our results suggest that Osh1 performs non-vesicular transport of ergosterol and PI(4)P at the NVJ.

INTRODUCTION

Membrane contact sites (MCSs) are hotspots for lipid exchange and cell signaling in eukaryotic cells. The close apposition of two membranes within the typical distance of 30 nm allows close tethering of proteins involved in these processes and a short distance for transport (Helle et al., 2013). The endoplasmic reticulum (ER) is the largest membrane-bound organelle in eukaryotic cells and it contacts with almost all types of subcellular organelles (Phillips and Voeltz, 2016). The ER synthesizes the majority of membrane lipids and distributes them to their final destinations by multiple mechanisms. Due to the hydrophobic nature of membrane lipids, their free diffusion through the aqueous cytosolic phase is very slow. Therefore, proper distribution of lipids between membranous organelles requires specialized transport pathways. Non-vesicular lipid transport, mediated by soluble carriers, is the major transport route for certain lipid types such as cholesterol and ceramide, between organelles that are not connected by membrane trafficking pathways (Prinz, 2010).

The oxysterol-binding protein (OSBP)-related proteins (ORPs) have been proposed as intracellular lipid transfer proteins, facilitating transport of sterols and other phospholipids between intracellular membranes (Mesmin and Antonny, 2016). Yeast contains 7 ORP genes (*OSH1-OSH7*), while humans possess 12 (Lehto et al., 2001). Many ORPs accumulate at contact sites between the ER and other subcellular membranes and promote the exchange of specific lipids, which helps to maintain a distinct membrane identity. The majority of ORPs in humans and the three Osh homologs in yeast contain multiple domains, such as the ankyrin repeat domain (ANK), GOLD, PH, and FFAT, in addition to the core OSBP-related domain (ORD) (Tong et al., 2016). The additional N-terminal PH, FFAT, and ANK domains are involved in membrane targeting by binding to specific membrane lipids or to membrane-anchored proteins (Raychaudhuri and Prinz, 2010). The ORPs are mainly localized in the cytosol, and the precise targeting of ORPs to subcellular membranes often requires the integration of multiple targeting modules. The lipid binding ORD domains contain the OSBP fingerprint motif EQVSHHPP and conserved basic residues, which recognize the head group of phosphatidylinositol 4-phosphate (PI(4)P). The binding of PI(4)P, as a primary ligand, is common for all ORPs and is essential for the ORP function (Tong et al., 2013). Many ORPs are experimentally confirmed to transport lipids between organellar membranes. They use a PI(4)P gradient as a driving force for the transport of secondary lipids such as sterols or phosphatidylserine (PS) (Chung et al., 2015; de Saint-Jean et al., 2011; Mesmin et al., 2013; Moser von Filseck et al., 2015a). Osh4 and OSBP can transfer sterol and PI(4)P in the opposite directions between two membranes, using the PI(4)P gradient as an energy source, which allows sterol transport against the concentration gradient (Mesmin et al., 2013; Moser von Filseck et al., 2015b). Osh6, ORP7, and ORP8 counter-transport PI(4)P and PS between the ER and the plasma membrane (Chung et al., 2015; Maeda et al., 2013; Moser von Filseck et al., 2015a). This directional transport of lipids is maintained by coupling with the PI(4)P hydrolysis by Sac1 phosphatase in the ER and the PI(4)P synthesis in the plasma membrane. So far, sterols and PS have been discovered as the secondary lipids transported by ORPs. The prediction of the ligand specificities of certain ORPs is not possible because of low sequence conservation of hydrophobic pockets and requires direct experimental characterization.

The perinuclear ER flattens around the cell nucleus to form the nuclear envelope as a double-membrane bilayer (Phillips and Voeltz, 2016). The perinuclear ER in yeast makes contact with vacuoles by forming nucleus-vacuole junctions (NVJs) by a Velcro-like association between the nuclear membrane protein Nvj1 and the vacuole membrane protein Vac8 (Kvam and Goldfarb, 2004). The NVJs mediate the piecemeal microautophagy of the nucleus (PMN) (Roberts et al., 2003). PMN is inhibited in yeast cells lacking all the Osh proteins, because of the loss of shared activity (Kvam and Goldfarb, 2004). Osh1 is recruited from cytoplasmic and Golgi pools into NVJs depending on the cellular level of Nvj1 (Kvam and Goldfarb, 2004). Yeast Osh1 contains three targeting domains, ANK, PH, and the FFAT motif in the N-terminal region. The ANK domain associates with Nvj1, which recruits Osh1 to the nuclear-vacuole junctions (Levine and Munro, 2001). The PH domain enables late Golgi targeting of Osh1 by interacting with phosphoinositide (Levine and Munro, 2001; Roy and Levine, 2004). Considering the general roles of ORPs, Osh1 appears to mediate lipid exchange at the MCSs including NVJs (Kvam and Goldfarb, 2004; Olkkonen and Levine, 2004). However, the secondary lipid transported by Osh1 is unknown, and the exact function of Osh1 at the NVJs is poorly understood.

To elucidate the key structural determinants for protein targeting to the NVJs, and the ligand specificities of Osh1, we determined the structures of ANK and ORD domains in complex with their cognate ligands, Nvj1 and ergosterol, respectively. The unique bi-lobed ANK structure allows association with Nvj1 in a cleft between the two subdomains. The structure of Osh1 ORD displays a conserved β-barrel fold, which accommodates PI(4)P as a primary ligand. We discovered that Osh1 ORD binds ergosterol as a secondary ligand. Competitive binding of PI(4)P and ergosterol, in a partially overlapping site, suggests that Osh1 functions as a PI(4)P/ergosterol exchanger. These data suggest that Osh1 is targeted to the NVJs by its N-terminal ANK domain and performs non-vesicular lipid transport by ergosterol/PI(4)P exchange.

RESULTS

Overall Structure of Osh1 ANK Domain

Osh1, one of the longest ORP members in yeast, has a conserved ORD domain in the C terminus and it contains N-terminal targeting modules, such as ANK, PH, and the FFAT motif. The ANK and PH domains are connected by a short linker spanning approximately ten amino acid residues (Figure 1A). In addition, Osh1 possesses a helical domain between the PH domain and the FFAT motif, which is predicted to contain short stretches of amphipathic helices. To elucidate the structural mechanisms governing the association of Osh1 ANK with the nuclear membrane protein Nvj1, we determined the crystal structures of ANK domains alone and in complex with the Nvj1 segment. The structure of the Osh1 ANK domain in *Kluyveromyces lactis* (KlOsh1 ANK) was determined by single anomalous dispersion phasing at 1.9 Å resolution (Table 1). The structure of the Osh1 ANK domain in *Saccharomyces cerevisiae* (ScOsh1 ANK) was solved at 1.5 Å resolution by molecular replacement using the structure of KlOsh1 ANK.

The ScOsh1 ANK domain is composed of 271 amino acids and contains seven repeats of two antiparallel α helices, followed by a long loop or a tight turn (Figure 1B). In typical ANK domains, the L-shaped consecutive repeats stack together to form an extended domain with a slight curvature. The ANK repeat generally contains the conserved TPLH tetrapeptide motif at the start of the inner α helix, which stabilizes ANK repeats through side chain hydrogen bonding between threonine and histidine residues (Mosavi et al., 2004). Except for the terminal repeats, each repeat contains the typical consensus sequence and forms a helix-turn-helix conformation. However, the ANK domain of Osh1 shows a substantial structural variation from the typical ANK domains. The Osh1 ANK domain displays a unique bi-lobed structure in which two ANK subdomains are connected by a central α helix (α8) (Figure 1C). The central helix α8 composes the last helix of the first subdomain and the starting helix of the second subdomain, resulting in a 180° rotational displacement of the second subdomain. This unusual configuration of the ANK domains creates two clefts around the central α helix, which may serve as binding pockets for the interacting proteins (Figure 1D). A structural similarity search in the PDB, using the DALI server, did not find ANK domains with a significant similarity to the Osh1 ANK, but found topologically related ANK domains in which two tandem ANK domains are connected by a central α helix (Figure S1).

The first and second subdomains in Osh1 ANK are composed of four ANK repeats and three ANK repeats, respectively. The Osh1 ANK domain contains only two signature motifs as TPLH at helix α8 and TVLH at helix α11. There are two four-residue 3_{10} helices between α7 and α8, and between α11 and α13. These two 3_{10} helices paired with α8 and α13, respectively, composes the C-terminal capping repeats of two ANK subdomains. If these small 3_{10} helices are considered as the helix components of ANK repeats, the helix pairs of ankyrin repeats are α1 + α2, α4 + α5, α6 + α7, 3_{10} + α8, α8 + α9, α11 + α12, and 3_{10} + α13, corresponding to the seven ankyrin repeats. The capping ANK repeat (α1 + α2) and the 3_{10} + α13 are structurally divergent from the typical ANK repeat. The typical hairpin loop following the first ANK repeat (α1 + α2) is missing and replaced by helix α3. The second 3_{10} helix and the long 3_{10}-α13 loop are relatively mobile with high B factors. While the Osh1 ANK contains features not observed in typical ANK repeat proteins, the overall ANK fold is preserved. The small 3_{10} helices of the C-terminal capping repeats of ANK domains were also observed in integrin-linked kinase and BRCA1-associated RING domain protein 1 (Chiswell et al., 2008; Fox et al., 2008) (Figure S1). The ANK domains of ScOsh1 and KlOsh1 show a structural conservation with a C_α root-mean-square deviation (RMSD) of 1.03 Å for the equivalent 213 residues. However, the seven ANK repeats in the second subdomain have flexible conformations with high B factors, and display a large structural variation between the ScOsh1 and KlOsh1 (Figure 1E).

Osh1 ANK Binds to the Small Cytosolic Segment of Nvj1

Nvj1 sequesters Osh1 to the NVJs in a Vac8-independent fashion by direct interaction with Osh1 ANK (Kvam and Goldfarb, 2004; Levine and Munro, 2001). The Osh1 binding site was mapped to the cytosolic segment (residues 130–177) of Nvj1 adjacent to the membrane-spanning region (Kvam and Goldfarb, 2006) (Figure 1A). To identify the core binding region of Nvj1, which is suitable for the X-ray crystallographic analysis of the Osh1 ANK-Nvj1

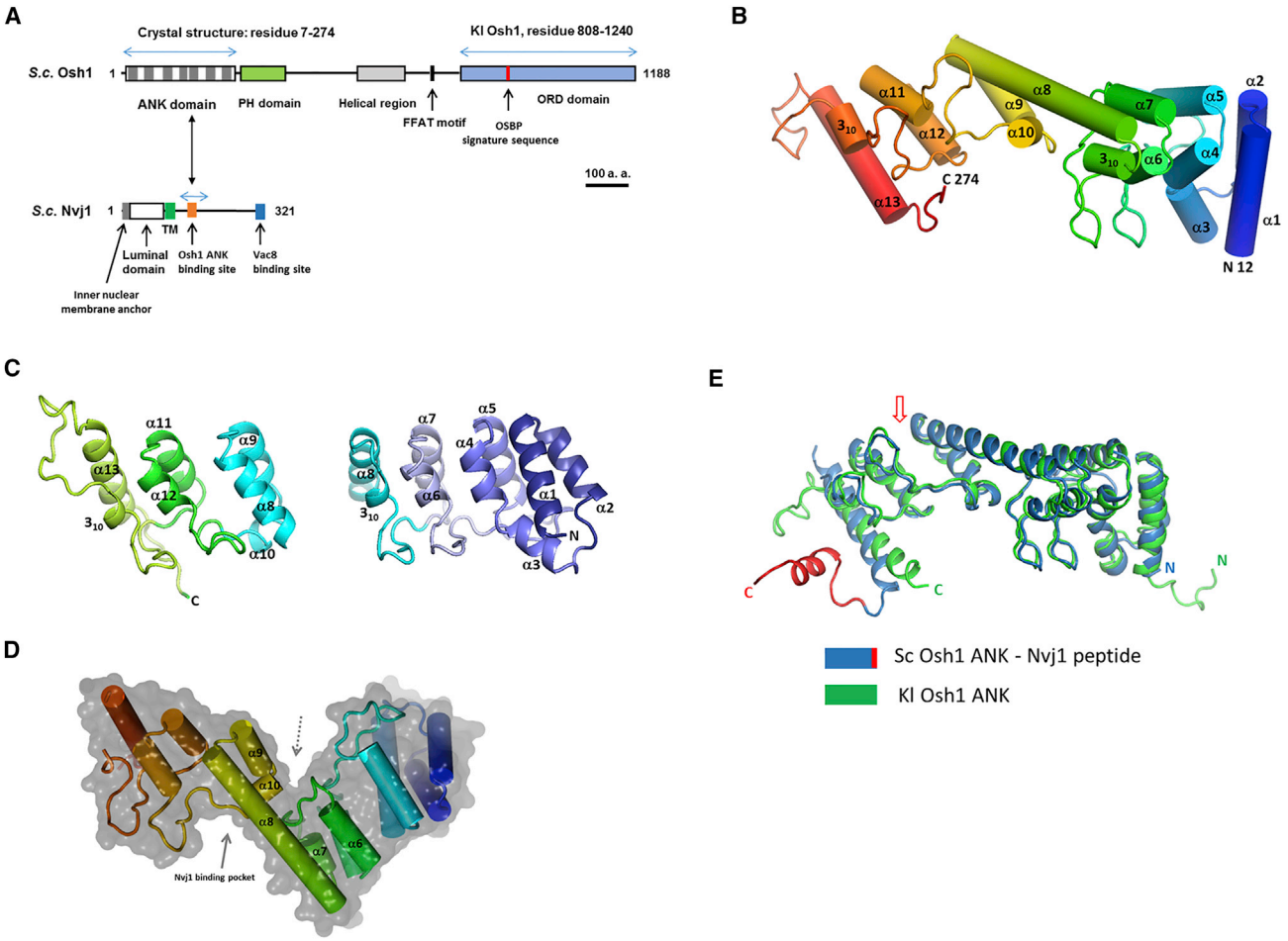

Figure 1. Overall Structure of Osh1 ANK

(A) Schematic representation of the domain structures of ScOsh1 and ScNvj1. The domains with the structures determined in this study are indicated with blue arrows. The seven ankyrin repeats are indicated as gray stripes on the ANK domain.

(B) The overall structure of the ScOsh1 ANK is shown in a cylindrical representation colored in blue to red for the N terminus to C terminus.

(C) Two subdomains connected by the helix α8 are shown individually with an equivalent orientation.

(D) The transparent surface is shown to indicate the two crevices in the ANK domain.

(E) Structural comparison of the ScOsh1 ANK and KlOsh1 ANK. Open arrow indicates the Nvj1 binding site.

See also Figures S1–S3.

complex, we performed the GST pull-down assay and co-elution of the ANK-Nvj1 complex in size-exclusion chromatography (SEC) using various truncation constructs of Nvj1. The smallest segment of Nvj1 required for Osh1 binding was determined to be the residues 139–156 (Figure 2). Yeast Nvj1 homologs in overall share low sequence similarity for the cytosolic region. However, the small Osh1-binding segment and the C-terminal Vac8-binding site are strictly conserved in yeast species, suggesting Osh1 targeting to the NVJs is a common theme in these homologs (Kvam and Goldfarb, 2006) (Figure S2).

Structure of the Osh1 ANK-Nvj1 Complex

To improve the crystallization properties of the Osh1 ANK-Nvj1 complex, we constructed a chimeric protein in which the Nvj1 segment (residues 139–165) is fused to the C terminus of Osh1 ANK domain. The formation of a stable Osh1 ANK-Nvj1 peptide complex appears to be more favorable when the ligand is near the protein as a C-terminal extension, rather than a free peptide in the solution. Apo Osh1 ANK is a monomer in solution when analyzed by SEC. The Osh1 ANK-Nvj1 chimera is a dimer, suggesting that the C-terminal Nvj1 segment of one protomer is bound to the ANK domain of the other protomer. The Osh1 ANK-Nvj1 was crystallized, and the diffraction data were collected at 3.5 Å resolution. The structure of the ANK-Nvj1 complex was solved by molecular replacement using the apo structure of ScOsh1 (Figure 3A). The electron densities of the Nvj1 segment bound to Osh1 were clearly visible for residues 139–153 (Figure S3). Previously, Levine and Munro (2001) proposed that the approximate Nvj1-binding site in Osh1 is the middle region of the ANK domain based on the examination of NVJ targeting of the chimeras composed of the Osh1 and Osh2 ANK fragments. This structural study reveals a detailed picture of the Osh1-Nvj1 interaction, which is consistent with the previous findings. The C-terminal Nvj1 sequence of Osh1 ANK associates

Table 1. Data Collection and Refinement Statistics

Crystal	KlOsh1 ANK	KlOsh1 ANK	ScOsh1 ANK	ScOsh1 ANK-Nvj1	KlOsh1 ORD– Ergosterol Complex	KlOsh1 ORD–Cholesterol Complex
Construct	residues 10–274, Se-Met	residues 10–274	residues 7–274	residues 7–274, 139–165	residues 808–1,240	esidues 808–1,240
Data collection	SAD	native	native	native	native	native
Beamline	PLS-7A	PLS-7A	PLS-7A	PLS-7A	PLS-5C	PLS-7A
Wavelength (Å)	0.97934 (peak)	0.97950	0.97950	0.97950	0.97950	0.97950
Space group	$P2_12_12$	$P2_12_12$	$P2_1$	$P2_12_12_1$	$P2_1$	$P2_1$
Unit cell parameters						
a, b, c (Å)	92.0, 189.6, 41.9	91.5, 189.1, 41.3	38.8, 55.0, 119.5	59.9, 67.7, 107.4	61.1, 47.2, 73.0	61.2, 46.6, 73.1
B(°)			95.1		96.2	96.3
Resolution limit (Å)	50–2.8 (2.85–2.80)	50–1.9 (1.93–1.90)	50–1.5 (1.50–1.53)	50–3.5 (3.56–3.50)	50–1.6 (1.63–1.60)	50–2.2 (2.24–2.20)
No. of reflections	87,787	547,746	327,744	43,097	220,699	61,174
No. of unique reflections	18,000 (862)	57,627 (2,821)	80,061 (3,964)	5,793 (274)	54,668 (2,718)	20,511 (991)
Multiplicity	4.9 (4.6)	9.5 (9.7)	4.1 (4.1)	7.4 (7.8)	4.0 (4.1)	3.0 (3.1)
Mean $I/\sigma(I)$	45.7 (17.6)	47.0 (9.7)	31.6 (4.8)	17.0 (7.3)	26.1 (5.3)	23.0 (5.2)
Completeness (%)	95.3 (98.0)	99.9 (100)	99.6 (99.0)	99.7 (100.0)	99.6 (99.2)	97.2 (97.0)
R_{merge} (%)	8.4 (15.6)	7.5 (46.0)	6.2 (37.1)	18.2 (41.5)	6.5 (30.6)	9.8 (37.3)
Wilson B factor (Å)	63.6	25.7	13.9	50.61	16.49	26.7
Refinement						
R_{work} (%)		17.9 (21.3)	18.4 (20.2)	18.4 (19.2)	17.7 (20.1)	19.1 (21.5)
R_{free} (%)		21.5 (24.7)	21.4 (24.1)	27.0 (30.1)	21.0 (24.4)	22.3 (25.2)
RMSD bond lengths (Å)		0.007	0.004	0.005	0.006	0.009
RMSD bond angles (°)		0.806	1.2	0.879	0. 905	1.038
B factor (Å^2)						
Overall		31.8	14.3	44.7	21.95	31.4
Molecule A (B)		26.5 (34.7)	12.5	44.7	20.6 (ergosterol 13.2)	31.4 (cholesterol 32.5)
Water (ions)		40.4	26.3	–	29.3 (SO_4 39.9)	34.4 (SO_4 57.0)
No. of non-H atoms						
Protein		4,191	2,254	2,145	3,440	3,434
Solvent		615	315	0	461	162
Ramachandran statistics (%)						
Favored		99.2	98.9	89.7	97.1	96.6
Disallowed		0	0	3	0	0
PDB:		5H2A	5H28	5H2C	5H2D	5WVR

Values in parentheses indicate the highest-resolution shell. RMSD, root-mean-square deviation; SAD, single anomalous dispersion.

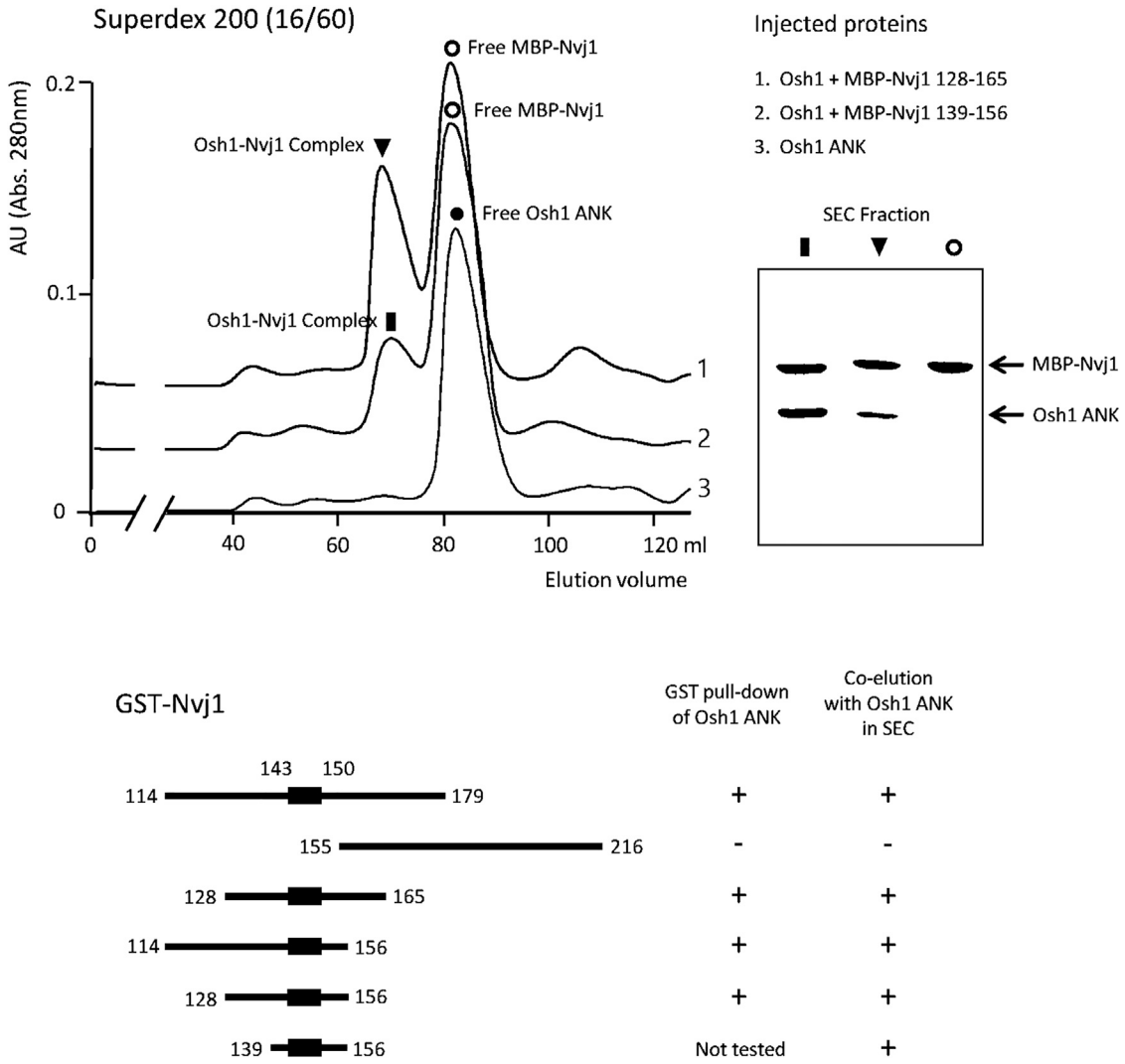

Figure 2. Osh1 ANK Binds to a Small Cytosolic Segment of Nvj1

Size-exclusion chromatography (SEC) profile of the Osh1 and Nvj1 mixture. Purified Osh1 ANK and various maltose-binding protein-fused Nvj1 constructs were mixed and loaded onto a size-exclusion column. A shematic summary of the GST pull-down assay and SEC analysis of the Osh1-ANK interaction is shown at the bottom. The Osh1 ANK bound to GST-Nvj1 was captured by GSH beads. The helix segment of Nvj1, visible in the crystal structure of Osh1-Nvj1, is shown in the gray rectangles.

with another symmetry-related molecule, forming continuous head-to-tail interactions in the crystal lattice (Figure 3B). The Nvj1 residues 143–152 form a 2.5 turn α helix and bind to the cleft between helix α8 and the α10-α11 loop of Osh1 ANK. The superposition of the apo and complex structures suggests that the first ANK subdomain has little structural changes, while the second subdomain undergoes a significant conformational change upon Nvj1 binding. In particular, the α10-α11 and α11-α12 loops move outward by 7.4 Å to form an open pocket and accommodate the helix segment of Nvj1 (Figure 3A).

The four hydrophobic residues (Tyr141, Val148, Leu149, and Phe151) and three hydrophilic residues of Nvj1 contribute to the Osh1-Nvj1 interface (Figure 3C). His140 and Arg146 of Nvj1 form salt bridges with Glu195 and Asp193 of Osh1, respectively. The side chain of Phe151 from Nvj1 inserts into the deep hydrophobic pocket located between α8 and the α10-α11 loop of Osh1 (Figure 3D). In the structure of KlOsh1 ANK, the N-terminal sequence, GSAMGS, originating from the multiple cloning site of the plasmid vector, associates with the Nvj1 binding site of a neighboring molecule in the asymmetric unit (Figure 3B). The N terminus of KlOsh1 interacts with the ANK domain as a pseudo-Nvj1 ligand by hydrogen bonds with the α10-α11 loop and by the hydrophobic interaction of Met4 with the Nvj1 binding pocket. The residues composing the Nvj1 binding site are well conserved in many fungal Osh1 homologs, suggesting that the association of ANK-Nvj1 is a common mode for NVJ targeting in these ORPs (Figure S2).

Nvj1 Binding to ANK Domain Is Specific to Osh1 Homolog

To confirm the protein interaction between Osh1 and Nvj1, the binding affinity of Osh1 ANK and the Nvj1 segment (residues 114–156) was measured by isothermal titration calorimetry

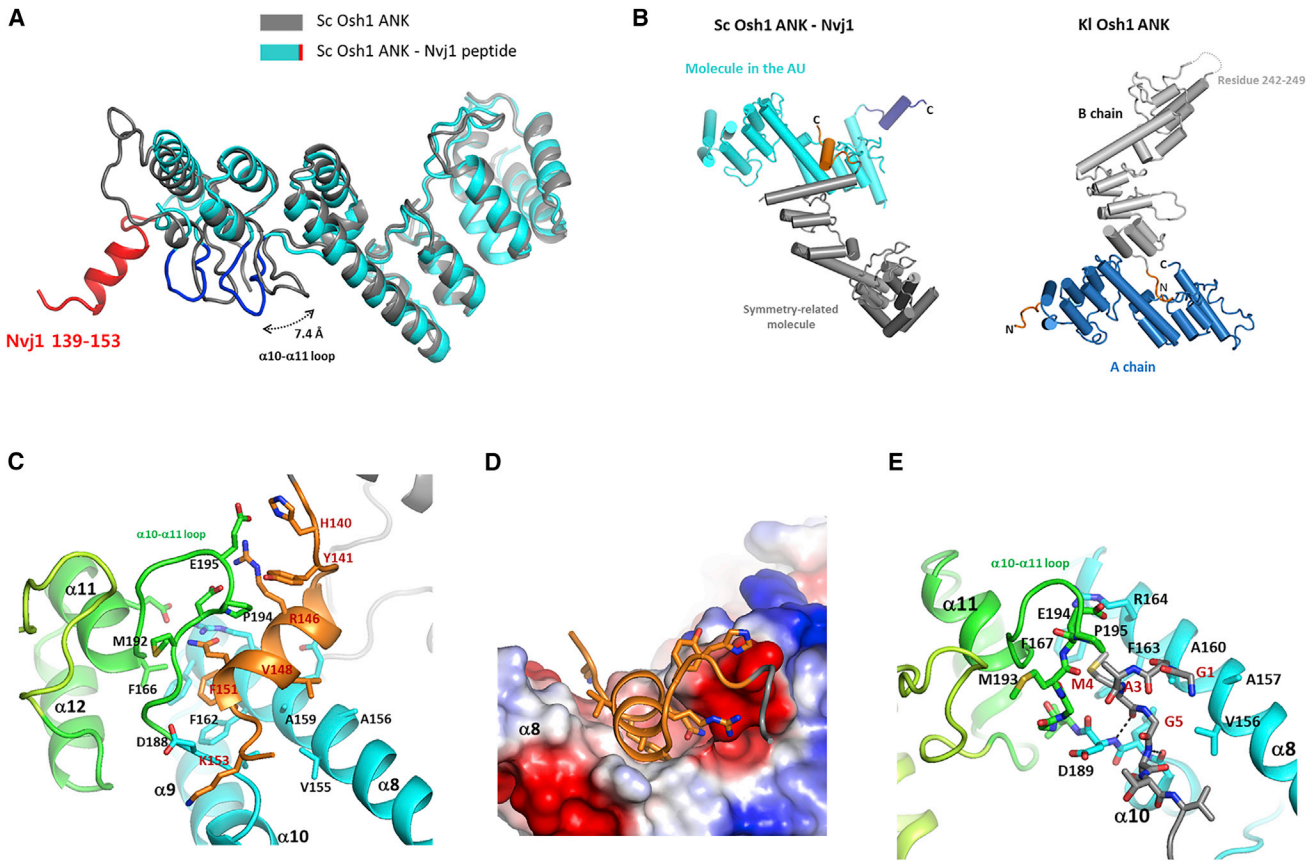

Figure 3. Structure of the Osh1 ANK-Nvj1 Complex

(A) Structure superposition of the apo ANK and Nvj1-bound ANK shows conformational changes in the Nvj1-binding site. The Nvj1 segment, fused to the C terminus of the ANK domain, is shown in red. The α10-α11 and α12-α13 loops of the Nvj1-bound Osh1 ANK are shown in blue to highlight the conformational change.

(B) Molecular interaction between the ScOsh1 ANK and the Nvj1 segment in the crystal lattice. The C-terminal Nvj1 sequence from the symmetry-related molecule associates with the ANK domain. The N-terminal segment of one protomer interacts with the Nvj1-binding site of the other protomer in the asymmetric unit of the KlOsh1 ANK crystal.

(C) The Nvj1-binding site of the ScOsh1 ANK. The Nvj1 segment (residues 140–153) is colored in orange.

(D) Surface representation of the ScOsh1 ANK-Nvj1 interaction. The Nvj1 segment is represented in cartoon and stick models.

(E) The Nvj1-binding site in the KlOsh1 ANK. The eight amino acids (GSAMGSTV) in the N terminus of KlOsh1 ANK are shown in the gray stick models.

See also Figures S2 and S3.

(ITC). The ScOsh1 ANK displayed a 1:1 binding stoichiometry, with an affinity of 10 μM K_d, to ScNvj1. The KlOsh1 ANK also binds to ScNvj1 with an affinity of 24 μM K_d, suggesting a conservation of Osh1-Nvj1 interaction in the different fungal species (Figure 4). In the Osh1-Nvj1 interface, the side chain of Ala159 in helix α8 of Osh1 fits into the space between Val148 and Phe151 of Nvj1 (Figure 3C). The mutation of Ala159 to any bulky residues in Osh1 is expected to interfere with the Osh1-Nvj1 interaction by steric clashes with Ala147 of Nvj1. As predicted, the Ala159Gln or Ala159Val mutation in the binding pocket of Osh1 ANK completely abolished the Nvj1 interaction, confirming that the protein-protein interaction observed in the crystal structure is consistent in solution (Figure 4). The association of Osh1 ANK and Nvj1 is weak, which allows both NVJ targeting and cytosolic distribution of Osh1.

S. cerevisiae has a close Osh1 paralog, Osh2, which arose from the whole-genome duplication (Beh et al., 2001). The functional domains of Osh1 and Osh2 are well conserved, with 84% sequence similarity for the ORD domains, and 68% similarity (49% identity) for the ANK domains. It was demonstrated that the ANK domain is necessary and sufficient for the targeting of Osh1 to the NVJ (Levine and Munro, 2001). However, Osh2 does not localize to the NVJs but distributes to the cytosol and plasma membranes (Levine and Munro, 2001). Consistently, the interaction of Osh2 ANK with Nvj1 was not detected in our ITC experiments (Figure 4). Sequence comparison of Osh1 and Osh2 shows that the Osh2 ANK has Val169, which corresponds to Ala159 in the Nvj1-binding pocket of Osh1 ANK (Figures S2 and 3C). The side chain of Val169 in Osh2 interferes with the Nvj1 binding by steric clashes, explaining the lack of NVJ localization of Osh2. The variation in the cellular targeting of Osh2 with the conserved ORD domain implies that Osh2 may have a similar lipid transport role in different intracellular locations.

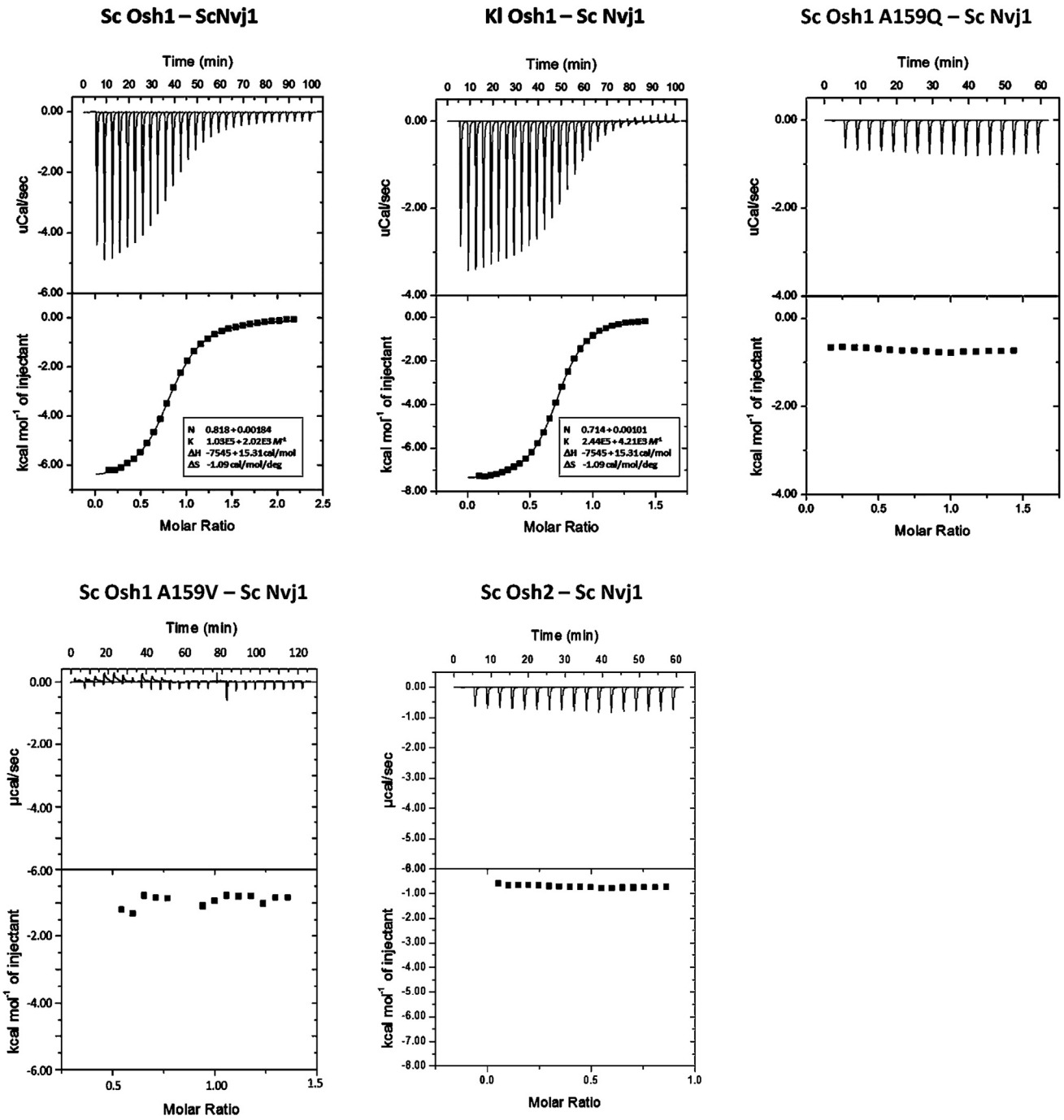

Figure 4. Analysis of the Osh1 ANK and Nvj1 Interaction by Isothermal Titration Calorimetry

The T4 lysozyme-Nvj1 (residues 114–156) fusion was placed in the cell and titrated by ANK domains loaded in the syringe. The titration data were fitted by the one-site binding model.

Osh1 ORD Binds PI(4)P and Ergosterol in a Mutually Exclusive Manner

All ORP homologs in eukaryotes contain a C-terminal ORD, which mediates the binding to several lipids such as PI(4)P, sterols, and PS (Tong et al., 2016). Recent evidence revealed that the unifying feature of all ORP homologs is the binding of PI(4)P as a primary ligand to the ORD domain (de Saint-Jean et al., 2011; Tong et al., 2013). Many ORPs are lipid transfer proteins, which exchange PI(4)P with a secondary lipid, such as sterol or PS, between organellar membranes (Tong et al., 2016). So far, the ligand specificities of many ORP homologs are known (Olkkonen, 2015). However, the secondary ligand for Osh1 is still unknown. Schulz et al. (2009) reported that the ORD domains of Osh2, Osh4, and Osh5 of *S. cerevisiae* transport sterols between

liposomes in vitro. However, the Osh1 ORD displayed little sterol transfer activity with a similar level to that of Osh3 ORD, which lacks sterol binding due to the narrow hydrophobic pocket (Schulz et al., 2009; Tong et al., 2013).

In this study, to confirm the sterol-binding properties of Osh1 ORD, we purified the ScOsh1 ORD using the *E. coli* expression system for in vitro sterol-binding experiments. We observed that the recombinant ScOsh1 ORD (residues 751–1,188) eluted in a void volume in SEC analysis, suggesting that the purified ScOsh1 ORD is aggregated. This may indicate protein misfolding, which explains the lack of ligand-binding properties of ScOsh1 ORD. To obtain homogeneous Osh1 ORD domain, we switched to the close Osh1 homologs from other fungal species. The Osh1 ORD of *K. lactis* displays 77% sequence similarity to the ScOsh1 ORD. The recombinant KlOsh1 ORD (residues 808–1,240), expressed in *E. coli*, formed aggregation, which is similar to the behavior of the ScOsh1 ORD. However, the addition of ergosterol or cholesterol to the culture medium during protein expression resolved the aggregation and resulted in monomeric distribution of KlOsh1 ORD in the SEC analysis. This indicates that ergosterol binding to the ORD domain stabilizes protein folding during protein expression.

To test whether KlOsh1 ORD directly binds to yeast sterols, we performed fluorescence resonance energy transfer-based sterol-binding assays using the purified ORD domain of KlOsh1. Dehydroergosterol (DHE), having intrinsic fluorescence properties, is similar to ergosterol in structural and chemical properties with a single double-bond difference. DHE can replace ergosterol in yeast without any functional interference (Mukherjee et al., 1998). The recombinant KlOsh1 ORD was purified in complex with ergosterol, which was added during cell culture and protein purification. To examine the DHE-binding property of KlOsh1 ORD, the purified protein was incubated with 2.5 μM DHE for 14 hr at 4°C. Competitive binding of DHE to the KlOsh1 ORD was expected to occur via replacement of the bound ergosterol. DHE binding was confirmed by monitoring the change in the fluorescence spectrum of the mixture when the tryptophan residues of the KlOsh1 ORD were excited at 285 nm. Spectral analysis revealed that tryptophan quenching at 340 nm was accompanied by the appearance of three emission peaks at 354, 373, and 393 nm (Figure 5A). These peaks are characteristic of DHE, which suggests the energy transfer from the KlOsh1 ORD to the bound DHE. Subsequently, the addition of DOPC:ergosterol (at a molar ratio of 2.3:1) liposomes to the DHE-bound KlOsh1 ORD eliminated the DHE fluorescence, suggesting that the KlOsh1 ORD exchanged the bound DHE for the ergosterol extracted from the liposomes.

To examine the PI(4)P/sterol exchange property of the Osh1 ORD, DHE fluorescence spectrum was monitored upon addition of excess soluble PI(4)P (3.2 μM) to the DHE-loaded Osh1 ORD. The significant reduction of the unique DHE spectrum upon PI(4)P addition suggests that PI(4)P replaced the sterol in the ligand-binding pocket of Osh1 ORD (Figure 5B). However, the addition of 6.0 μM of 1-palmitoyl-2- oleoyl-*sn*-glycero-3-phospho-l-serine (POPS) to the DHE-loaded Osh1 ORD did not change the DHE fluorescence spectrum, suggesting that the Osh1 ORD does not bind PS. In conclusion, these data suggest that the Osh1 ORD binds ergosterol as a second ligand and transfers lipids as a PI(4)P/sterol exchanger.

Structure of Osh1 ORD-Sterol Complex

To identify the structural determinants of sterol recognition by Osh1, we solved the crystal structures of the Osh1 ORD from *K. lactis* in complex with ergosterol and cholesterol at 1.6 and 2.2 Å resolutions, respectively. The structures of KlOsh1 ORD were solved by molecular replacement using the ScOsh3 ORD as the search model (Tong et al., 2013). The structure of KlOsh1 ORD is composed of 9 α helices and 18 β strands, and displays an incomplete β barrel with a central ligand-binding tunnel and a lid covering the tunnel entrance (Figure 5C). The KlOsh1 ORD contains a flexible loop insertion composed of 28 residues at β15-β16 compared with other Osh homologs (Figure S4). In addition, the KlOsh1 ORD contains one additional helix (α1) at the N terminus of the ORD domain. The helix α1 is followed by an extended loop, which is connected to the lid covering the ligand-binding tunnel. The residues in the interface of helix α1 and the core β barrel are conserved in KlOsh1 and ScOsh1, while the solvent-exposed residues are variable, suggesting that ScOsh1 also contains the equivalent helix α1. Despite these variations in the structures of the ORD domains, the overall structure of the KlOsh1 ORD is conserved in ORP members, displaying a C_α RMSD of 1.1 Å to ScOsh3 ORD which has a 44% sequence similarity to KlOsh1 ORD (Figure 5D).

The residues composing the binding site of the PI(4)P head group are strictly conserved in all ORP members (Figure S4). The structure superposition of the Osh1 ORD and Osh3 ORD shows that the conserved "OSBP fingerprint motif" and the basic residues around the tunnel entrance have almost identical conformations (Figure 5E). The structures of Osh3-PI(4)P (Tong et al., 2013), Osh4-PI(4)P (de Saint-Jean et al., 2011), and Osh6-PI(4)P (Moser von Filseck et al., 2015a) show that the binding pockets are complementary to the PI(4)P head group, suggesting that phosphatidylinositol phosphates (PIPs) other than PI(4)P are not allowed. For example, the 5- and 6-phosphate groups in the inositol ring of PIPs sterically clash with helix α8. The N-terminal lid in a closed conformation clashes with the 3-phosphate group of PIPs. We did not test the binding of PIPs other than PI(4)P in this study. However, the identical structures of the PI(4)P-binding sites in all ORPs suggest that they share the specificity toward PIPs.

The $2F_o–F_c$ maps at 1.6 and 2.2 Å resolutions show clear electron densities of a bound sterol and water molecules accommodated in the hydrophobic tunnel (Figure S3). The closed conformation of the lid creates a sealed hydrophobic tunnel with a volume of 880 $Å^3$ (Figure 6A). The upper part of the tunnel wall is composed of 15 hydrophobic residues and the tunnel bottom has nine polar residues. The hydroxyl group of sterol forms hydrogen bonds with the side chains of Asp881 (3.1 Å) and Lys1007 (2.8 Å), which compose the polar clusters at the tunnel bottom (Figure 6B). The cholesterol-bound form of the Osh1 ORD has a virtually identical structure to the ergosterol-bound form. Cholesterol is accommodated in the hydrophobic pocket in a configuration identical to that of ergosterol (Figure 6C).

Previously, the structures of Osh4 in complex with various sterol ligands (ergosterol, cholesterol, 25-hydroxycholesterol, 20-hydroxycholesterol, and 7-hydroxycholesterol) revealed that a

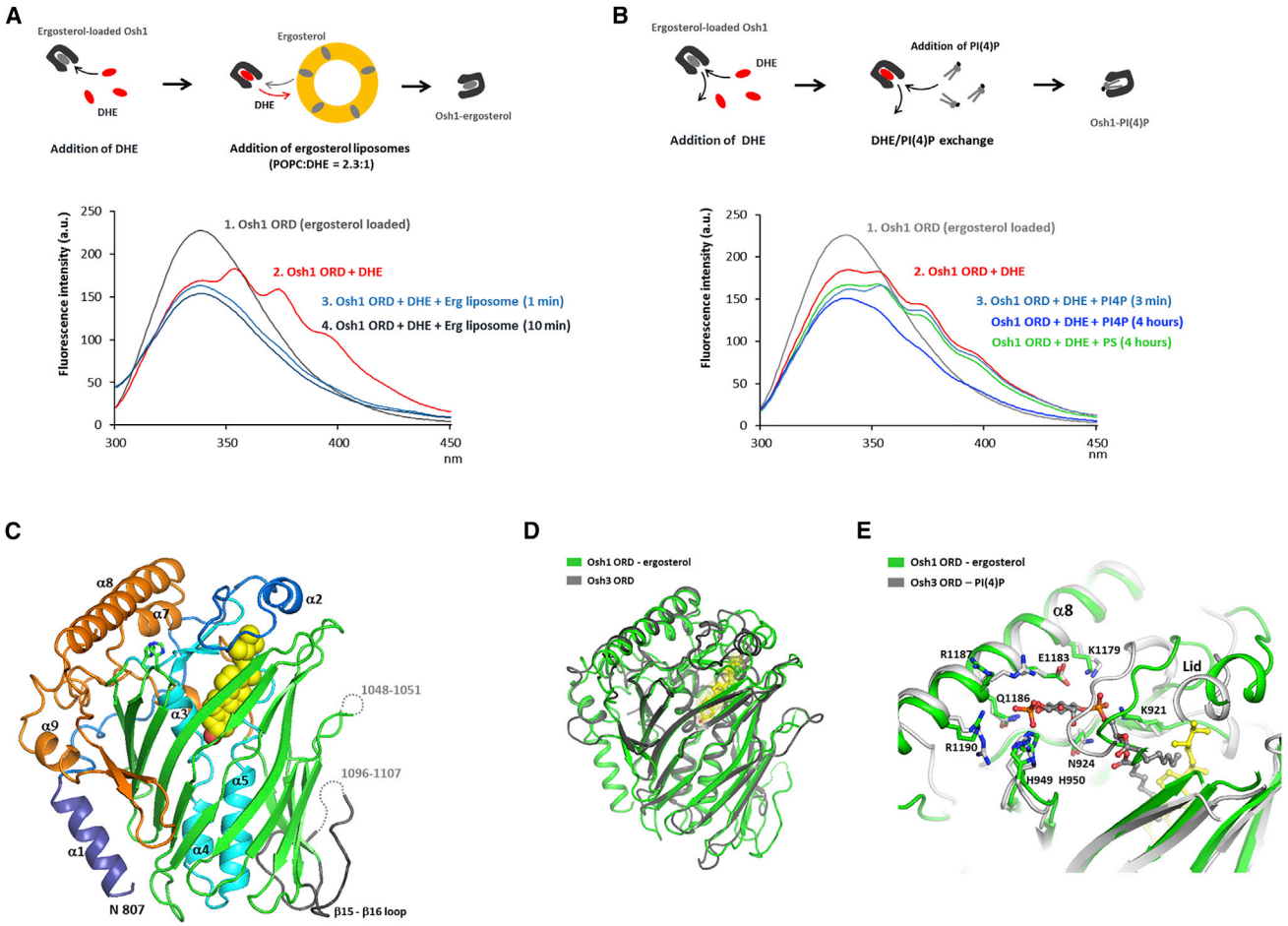

Figure 5. Ergosterol and PI(4)P Binding by the Osh1 ORD and the Structure of the Osh1 ORD-ergosterol Complex

(A) Measurement of ergosterol/DHE binding to the Osh1 ORD by fluorescence resonance energy transfer techniques. A cartoon representation shows the experimental strategy. The recombinant KlOsh1 ORD was purified in complex with ergosterol (spectrum 1). The addition of DHE (2.5 μM) to the ergosterol-loaded Osh1 ORD (protein concentration of 1.0 μM) led to an increase in fluorescence emission at 375 nm, indicating the competitive binding of DHE to the Osh1 ORD (spectrum 2). Subsequent addition of ergosterol-loaded liposomes (at a molar ratio of DOPC:DHE of 2.3:1) to the sample eliminated the DHE fluorescence, indicating that non-fluorescent ergosterol replaced the bound DHE in the Osh1 ORD (spectra 3 and 4).

(B) DHE/PI(4)P exchange activity was examined by monitoring the changes in the fluorescence spectrum after the addition of soluble PI(4)P diC8 to the DHE-loaded Osh1 ORD. DHE was loaded to Osh1 by incubating with 2.5 μM of DHE for 14 hr at 4°C. Then, 3.2 μM of PI(4)P was added to the sample, and the spectra were measured after 3 min and 4 hr. Next, 6.0 μM of POPS was added to the DHE-loaded Osh1 ORD, and the spectrum was measured after 4 hr.

(C) The overall structure of the KlOsh1 ORD. The bound ergosterol is shown in sphere models. The ORD domain is colored in blue, cyan, green, and orange for the N-terminal lid (residues 807–866), central α helices (867–926), β barrel (927–1,126), and the C-terminal subdomain (1,127–1,240), respectively. The β15-β16 loop is shown in dark gray.

(D) Structure superposition of the Osh1 ORD and Osh3 ORD.

(E) Comparison of the PI(4)P-binding sites of Osh1 and Osh3 shows strict conservation of residues involved in the recognition of the PI(4)P head group.

See also Figure S4.

sterol molecule is accommodated in the hydrophobic tunnel with the 3-hydroxyl group of the sterol oriented toward the polar clusters at the tunnel bottom and the hydrophobic backbones of the sterol contacting the tunnel wall (Im et al., 2005). The residues involved in sterol recognition by Osh4 are poorly conserved in ORP homologs except for the closest homolog Osh5, which made it difficult to predict the ligand specificities of other Osh homologs (Figure S4). Although the residues in the sterol-binding pockets of Osh1 and Osh4 are not well conserved, both homologs accommodate sterols in a head-down orientation with hydrogen bonds between the 3-hydroxyl group of the sterol and the polar residues at the tunnel bottom. However, Osh1 and Osh4 display a different binding angle of sterol molecules. Ergosterol is accommodated in Osh1 with a 180°rotation along its long axis compared with the binding mode of Osh4 (Figure 6D). Considering the rigidity of sterol molecules, the different shapes of the binding pockets may contribute to the specific orientations of sterols in the binding pockets of Osh1 and Osh4. Osh1 and Osh4 possess a cavity volume large enough to accommodate a single ergosterol and additional water molecules, which explains the promiscuous binding to various sterol ligands (Im et al., 2005).

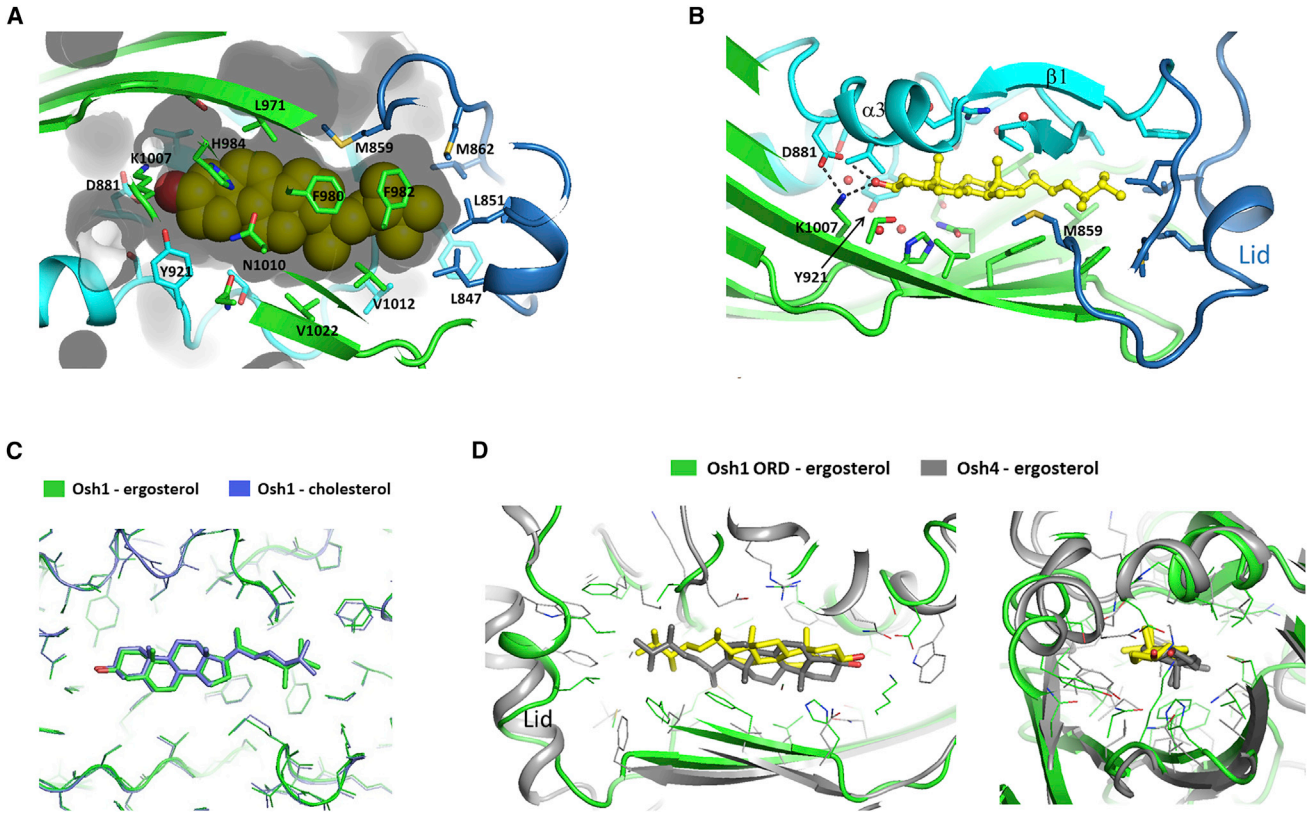

Figure 6. Sterol-Binding Pocket of the Osh1 ORD

(A) Surface representation of the hydrophobic pocket. The residues composing the tunnel wall are shown as sticks. The transparent surface of the sterol-binding cavity is shown.

(B) Sterol-binding pocket of the Osh1 ORD. Ergosterol and six water molecules in the tunnel are shown in ball and stick models.

(C) Structure superposition of the Osh1 ORDs in complex with ergosterol and cholesterol.

(D) Comparison of the ergosterol-binding modes of Osh1 and Osh4 by superposition of the ORD domains. The residues composing the sterol-binding cavity are shown as lines.

See also Figures S3 and S4.

DISCUSSION

The vacuole as a primary storage compartment in yeasts is a key organelle involved in non-specific intracellular proteolysis and protein trafficking (Li and Kane, 2009). Yeast vacuoles are dynamic structures that exist as single large compartments or as several smaller compartments. Although sterols are not abundant in the vacuolar membranes (Zinser and Daum, 1995; Zinser et al., 1993), ergosterol is essential for the priming step in homotypic vacuole fusion, and a lack of ergosterol leads to vacuole fragmentation (Hongay et al., 2002; Kato and Wickner, 2001). Vacuole fusion requires ergosterol, diacylglycerol, PI(3)P, and PI(4)P as regulatory lipids, which interdependently congregate at the vertices of fusing membranes, and are necessary for the enrichment of other factors such as SNAREs, Ypt7p1, and HOPS (Fratti et al., 2004; Kato and Wickner, 2001; Li and Kane, 2009). The vacuole contacts the perinuclear ER membrane, forming an NVJ by a Velcro-like association between Nvj1 and Vac8 (Kvam and Goldfarb, 2004). NVJs mediate the PMN, which involves the pinching off of non-essential portions of the nucleus into invaginations of the vacuole membrane for degradation (Roberts et al., 2003). Osh-depleted cells accumulate PMN structures and show reduced PMN-mediated degradation (Kvam and Goldfarb, 2004). Therefore, the spatiotemporal change of sterol and phosphoinositide contents in the vacuolar membrane seem to have a significant influence on the membrane properties, which are important for membrane sorting and trafficking processes. This suggests the existence of an efficient lipid transport pathway to control the sterol and phosphoinositide levels at the localized vacuole membranes.

In this study, we identified the Nvj1-Osh1 interaction, and determined the structures of ANK and ORD in complex with their cognate ligands, to reveal the key determinants for protein targeting and lipid transport at the NVJs. Based on these findings, we propose that Osh1 counter-transports ergosterol and PI(4)P between the perinuclear ER and vacuolar membranes. The Osh1 ANK displays a bi-lobed structure, with an Nvj1-binding cleft between the two subdomains, and recognizes the small cytosolic segment of Nvj1. The Nvj1-binding site in Osh1 and the helix segment of Nvj1 are well preserved in many fungal Osh homologs, implying that NVJ targeting of Osh1 is a common theme in these species. Osh2 has an identical domain

organization and high sequence similarity to Osh1, but has a variation of the key residue in the Osh2 ANK that interferes with Nvj1 binding. The difference in the ANK domains correlates with the diffuse cytoplasmic and plasma membrane distribution of Osh2 (Levine and Munro, 2001). Considering the high sequence conservation of ORD domains between Osh1 and Osh2, these Osh homologs may play a similar role in lipid transport at spatially distinct locations. Currently, the binding partner of the Osh2 ANK is unknown, and further investigation is required to delineate whether the Osh2 ANK uses an equivalent Nvj1-binding site for interacting with another protein with different ligand specificities.

The presence of the ANK domain is not limited to yeast ORP homologs. Human ORP1 contains an N-terminal ANK domain (residues 1–237), which contributes to the late endosomal localization (Johansson et al., 2003). The endosomal targeting of ORP1 is mediated by the interaction between its ANK domain and the GTP-bound form of Rab7, which is anchored to the endosomal membranes. This ORP1-Rab7 interaction is known to regulate the mobility and distribution of late endosomes via connection to the Rab7-interacting lysosomal protein and dynein/dynactin motor complexes (Johansson et al., 2005, 2007; Rocha et al., 2009; van der Kant et al., 2013). The sequence homology of Osh1 ANK and ORP1 ANK is very low, and the binding partners for these ANK domains are functionally independent. However, the ANK domains of human and yeast ORPs are involved in protein targeting to specific subcellular membranes by their unique protein-protein interactions, which allows the ORPs to perform non-vesicular lipid transport at the MCSs.

Recently, significant advances have been made in understanding the molecular mechanism of lipid transport by ORPs. Many ORPs, such as Osh4, OSBP, Osh6, ORP5, and ORP8, exchange PI(4)P with a secondary lipid, such as sterols or PS, between organellar membranes (Chung et al., 2015; de Saint-Jean et al., 2011; Maeda et al., 2013; Mesmin et al., 2013; Moser von Filseck et al., 2015a). The transport of secondary lipids against their concentration gradient is powered by using the PI(4)P gradient as an energy source. All ORPs bind PI(4)P as a primary ligand in the conserved pocket of the C-terminal ORD domain (de Saint-Jean et al., 2011; Tong et al., 2013). The secondary lipid binds to the ORD in the partially overlapping binding site with the PI(4)P, which allows only one lipid binding at a time. Considering the conservation of general domain architecture in ORPs, the major roles of ORPs seems to be the PI(4)P-coupled transport of various secondary lipids from the ER to other organellar membranes (Mesmin and Antonny, 2016; Moser von Filseck and Drin, 2016).

S. cerevisiae contains seven ORP homologs, Osh1-Osh7, which are divided into four subclasses based on sequence conservation. Osh1 and its close homolog Osh2 compose the first subgroup of Osh proteins. The structures of ORD domains have been reported only for Osh3, Osh4, and Osh6, each representing one of the three different subgroups (Im et al., 2005; Maeda et al., 2013; Tong et al., 2013). This study reports on the structure of the Osh1 ORD, which completes the structural views on the representative members of all the Osh homologs. The structure of Osh1 shows that the overall folds of the ORD domains and the configuration of PI(4)P-binding sites are well conserved in ORP members. We discovered by structural study and ligand-binding assays that the secondary ligand for Osh1 is ergosterol. Four out of seven Osh homologs in yeast (Osh1, Osh2, Osh4, and Osh5) display different cellular distributions, but are commonly involved in the PI(4)P-dependent transport of ergosterol between two membranes, which is consistent with the original reports on the role of Osh proteins in the sterol homeostasis of yeast cells (Beh et al., 2001; Beh and Rine, 2004). Osh6 and Osh7 transport PS as a secondary ligand. We did not observe a PS-binding activity of the Osh1 ORD. Consistently, structural comparison with the PS-bound Osh6 shows that the residues involved in the PS recognition are not well conserved in Osh1. Modeling of PS into the Osh1 ORD shows that Met859 (in the N-terminal lid), Phe980 (β7), and Phe982 (β7) clash with the *sn*-2 acyl group of PS, suggesting that Osh1 may not bind PS.

MCSs are closely apposed regions, where membranes of two organelles come into close proximity, typically within 30 nm (Levine and Loewen, 2006). The domain architecture of Osh1 correlates with the ability to transfer lipids, optimized at the MCSs, such as NVJs and the ER-Golgi interface. The intracellular localization of Osh1 seems to be not dominated by a single targeting module, but rather determined by integration of multiple interactions, which explains the diffusible properties of Osh1 between cytosolic and membrane localizations. Overall, the structure of Osh1 is consistent with the bridge and shuttle model of ORPs. In this model, the N-terminal targeting modules interact with two different membranes in the MCSs, while the ORD domain, connected to the N-terminal domains by long flexible loops, shuttles lipids between the membranes. The loop connecting the ANK-PH and the FFAT motif in Osh1 is composed of 300 residues roughly corresponding to 75 nm in length when calculated using the average C_α distance of 2.5 Å between two consecutive residues. The flexible loop, connecting the FFAT motif and the ORD, is approximately 40 residues, which covers a distance of 10 nm. Therefore, Osh1 may either shuttle across the MCSs, or transport lipids by bridging the MCS, which would increase the efficiency of lipid transfer.

In conclusion, we summarize the role of Osh1 at the NVJ (Figure 7). The NVJs in yeast are formed by the association between the nuclear membrane protein Nvj1 and the vacuole membrane protein Vac8 (Kvam and Goldfarb, 2004). Osh1 localizes to the NVJs by the association of multiple targeting domains with specific lipids, or proteins, localized at the NVJs. The Osh1 PH associates with the PI(4)P in the vacuole membranes (Fratti et al., 2004). The ANK domain in Osh1 binds to the cytosolic segment of Nvj1. The FFAT motif associates with the MSP domain of the vesicle-associated membrane protein-associated protein in the ER membrane (Murphy and Levine, 2016). The ORD domain performs lipid transport by the PI(4)P/ergosterol exchange between the membranes, thereby influencing the sterol/PI(4)P balance in the localized vacuole and perinuclear ER membranes. Further investigations are required to determine the regulatory mechanism of Osh1-mediated lipid transport at the NVJs in accordance with the vacuolar requirements.

STAR★METHODS

Detailed methods are provided in the online version of this paper and include the following:

- KEY RESOURCES TABLE
- CONTACT FOR REAGENT AND RESOURCE SHARING

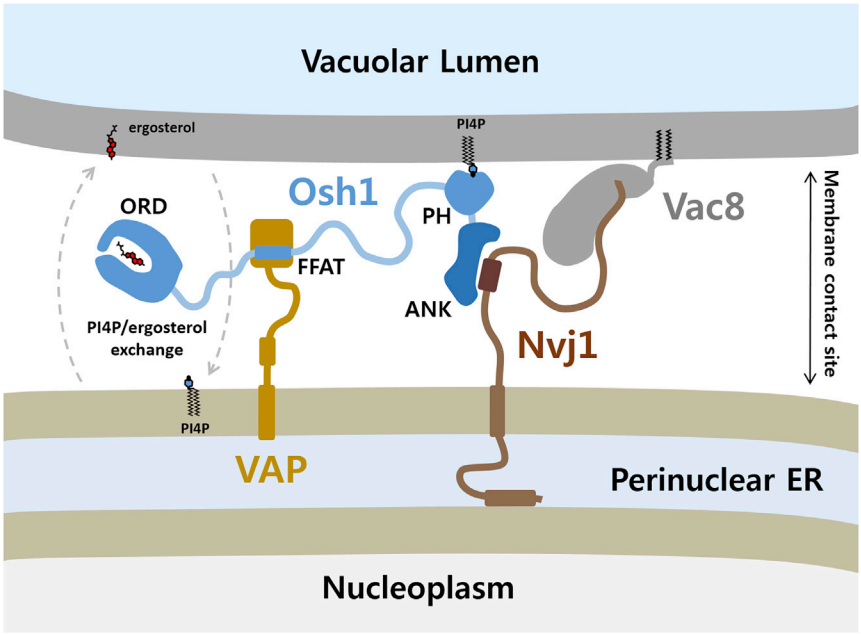

Figure 7. Schematic Model of the Osh1 Function at the Membrane Contact Site
Osh1 localizes to NVJs by the association of ANK, PH, and the FFAT motif with the nuclear membrane protein Nvj1 and PI(4)P on the vacuole membrane, and the vesicle-associated membrane protein-associated protein (VAP) in the perinuclear ER, respectively. The ORD domain counter-transports PI(4)P and ergosterol between the membranes.

- METHOD DETAILS
  - Cloning of Yeast Osh1 ANK and ORD Domains
  - Construction of Osh1 ANK–Nvj1 Chimera
  - Protein Expression and Purification
  - Crystallization and Crystallographic Analysis
  - Isothermal Titration Calorimetry of the Osh1 ANK-Nvj1 Interaction
  - Preparation of the Liposomes
  - Sterol and PI(4)P Binding Assays Using FRET

SUPPLEMENTAL INFORMATION

Supplemental Information includes four figures and can be found with this article online at http://dx.doi.org/10.1016/j.str.2017.02.010.

AUTHOR CONTRIBUTIONS

Y.J.I. and M.K.M. designed the project; M.K.M., J.T., and H.Y. cloned the genes, and purified and crystallized the recombinant proteins; M.K.M. and J.T. performed the ligand-binding assays; M.K.M., J.T., H.Y., and Y.J.I. collected the X-ray data and performed structure refinements; Y.J.I. wrote the manuscript. All authors discussed the results and approved the manuscript.

ACKNOWLEDGMENTS

This project was supported by a grant from the National Research Foundation of Korea (NRF) funded by the Ministry of Education, Science and Technology (grant nos. NRF-2014R1A1A1003060 and 2015M2B2A4031729). This study was financially supported by the research program of the Chonnam National University (grant no. 2012-0213 to Y.J.I.).

Received: October 28, 2016
Revised: January 19, 2017
Accepted: February 22, 2017
Published: March 16, 2017

REFERENCES

Adams, P.D., Afonine, P.V., Bunkoczi, G., Chen, V.B., Davis, I.W., Echols, N., Headd, J.J., Hung, L.W., Kapral, G.J., Grosse-Kunstleve, R.W., et al. (2010). PHENIX: a comprehensive Python-based system for macromolecular structure solution. Acta Crystallogr. D Biol. Crystallogr. *66*, 213–221.

Beh, C.T., and Rine, J. (2004). A role for yeast oxysterol-binding protein homologs in endocytosis and in the maintenance of intracellular sterol-lipid distribution. J. Cell Sci. *117*, 2983–2996.

Beh, C.T., Cool, L., Phillips, J., and Rine, J. (2001). Overlapping functions of the yeast oxysterol-binding protein homologues. Genetics *157*, 1117–1140.

Chiswell, B.P., Zhang, R., Murphy, J.W., Boggon, T.J., and Calderwood, D.A. (2008). The structural basis of integrin-linked kinase-PINCH interactions. Proc. Natl. Acad. Sci. USA *105*, 20677–20682.

Chung, J., Torta, F., Masai, K., Lucast, L., Czapla, H., Tanner, L.B., Narayanaswamy, P., Wenk, M.R., Nakatsu, F., and De Camilli, P. (2015). Intracellular transport. PI4P/phosphatidylserine countertransport at ORP5- and ORP8-mediated ER-plasma membrane contacts. Science *349*, 428–432.

de Saint-Jean, M., Delfosse, V., Douguet, D., Chicanne, G., Payrastre, B., Bourguet, W., Antonny, B., and Drin, G. (2011). Osh4p exchanges sterols for phosphatidylinositol 4-phosphate between lipid bilayers. J. Cell Biol. *195*, 965–978.

Doublie, S. (1997). Preparation of selenomethionyl proteins for phase determination. Methods Enzymol. *276*, 523–530.

Emsley, P., Lohkamp, B., Scott, W.G., and Cowtan, K. (2010). Features and development of Coot. Acta Crystallogr. D Biol. Crystallogr. *66*, 486–501.

Fox, D., 3rd, Le Trong, I., Rajagopal, P., Brzovic, P.S., Stenkamp, R.E., and Klevit, R.E. (2008). Crystal structure of the BARD1 ankyrin repeat domain and its functional consequences. J. Biol. Chem. *283*, 21179–21186.

Fratti, R.A., Jun, Y., Merz, A.J., Margolis, N., and Wickner, W. (2004). Interdependent assembly of specific regulatory lipids and membrane fusion proteins into the vertex ring domain of docked vacuoles. J. Cell Biol. *167*, 1087–1098.

Helle, S.C., Kanfer, G., Kolar, K., Lang, A., Michel, A.H., and Kornmann, B. (2013). Organization and function of membrane contact sites. Biochim. Biophys. Acta *1833*, 2526–2541.

Hongay, C., Jia, N., Bard, M., and Winston, F. (2002). Mot3 is a transcriptional repressor of ergosterol biosynthetic genes and is required for normal vacuolar function in *Saccharomyces cerevisiae*. EMBO J. *21*, 4114–4124.

Im, Y.J., Raychaudhuri, S., Prinz, W.A., and Hurley, J.H. (2005). Structural mechanism for sterol sensing and transport by OSBP-related proteins. Nature *437*, 154–158.

Johansson, M., Bocher, V., Lehto, M., Chinetti, G., Kuismanen, E., Ehnholm, C., Staels, B., and Olkkonen, V.M. (2003). The two variants of oxysterol binding protein-related protein-1 display different tissue expression patterns, have different intracellular localization, and are functionally distinct. Mol. Biol. Cell *14*, 903–915.

Johansson, M., Lehto, M., Tanhuanpaa, K., Cover, T.L., and Olkkonen, V.M. (2005). The oxysterol-binding protein homologue ORP1L interacts with Rab7 and alters functional properties of late endocytic compartments. Mol. Biol. Cell *16*, 5480–5492.

Johansson, M., Rocha, N., Zwart, W., Jordens, I., Janssen, L., Kuijl, C., Olkkonen, V.M., and Neefjes, J. (2007). Activation of endosomal dynein motors by stepwise assembly of Rab7-RILP-p150Glued, ORP1L, and the receptor betalll spectrin. J. Cell Biol. *176*, 459–471.

Kato, M., and Wickner, W. (2001). Ergosterol is required for the Sec18/ATP-dependent priming step of homotypic vacuole fusion. EMBO J. *20*, 4035–4040.

Kvam, E., and Goldfarb, D.S. (2004). Nvj1p is the outer-nuclear-membrane receptor for oxysterol-binding protein homolog Osh1p in *Saccharomyces cerevisiae*. J. Cell Sci. *117*, 4959–4968.

Kvam, E., and Goldfarb, D.S. (2006). Structure and function of nucleus-vacuole junctions: outer-nuclear-membrane targeting of Nvj1p and a role in tryptophan uptake. J. Cell Sci. *119*, 3622–3633.

Lehto, M., Laitinen, S., Chinetti, G., Johansson, M., Ehnholm, C., Staels, B., Ikonen, E., and Olkkonen, V.M. (2001). The OSBP-related protein family in humans. J. Lipid Res. *42*, 1203–1213.

Levine, T., and Loewen, C. (2006). Inter-organelle membrane contact sites: through a glass, darkly. Curr. Opin. Cell Biol. *18*, 371–378.

Levine, T.P., and Munro, S. (2001). Dual targeting of Osh1p, a yeast homologue of oxysterol-binding protein, to both the Golgi and the nucleus-vacuole junction. Mol. Biol. Cell *12*, 1633–1644.

Li, S.C., and Kane, P.M. (2009). The yeast lysosome-like vacuole: endpoint and crossroads. Biochim. Biophys. Acta *1793*, 650–663.

Maeda, K., Anand, K., Chiapparino, A., Kumar, A., Poletto, M., Kaksonen, M., and Gavin, A.C. (2013). Interactome map uncovers phosphatidylserine transport by oxysterol-binding proteins. Nature *501*, 257–261.

Mesmin, B., and Antonny, B. (2016). The counterflow transport of sterols and PI4P. Biochim. Biophys. Acta *1861*, 940–951.

Mesmin, B., Bigay, J., Moser von Filseck, J., Lacas-Gervais, S., Drin, G., and Antonny, B. (2013). A four-step cycle driven by PI(4)P hydrolysis directs sterol/PI(4)P exchange by the ER-Golgi tether OSBP. Cell *155*, 830–843.

Mosavi, L.K., Cammett, T.J., Desrosiers, D.C., and Peng, Z.Y. (2004). The ankyrin repeat as molecular architecture for protein recognition. Protein Sci. *13*, 1435–1448.

Moser von Filseck, J., and Drin, G. (2016). Running up that hill: how to create cellular lipid gradients by lipid counter-flows. Biochimie *130*, 115–121.

Moser von Filseck, J., Copic, A., Delfosse, V., Vanni, S., Jackson, C.L., Bourguet, W., and Drin, G. (2015a). Intracellular transport. Phosphatidylserine transport by ORP/Osh proteins is driven by phosphatidylinositol 4-phosphate. Science *349*, 432–436.

Moser von Filseck, J., Vanni, S., Mesmin, B., Antonny, B., and Drin, G. (2015b). A phosphatidylinositol-4-phosphate powered exchange mechanism to create a lipid gradient between membranes. Nat. Commun. *6*, 6671.

Mukherjee, S., Zha, X., Tabas, I., and Maxfield, F.R. (1998). Cholesterol distribution in living cells: fluorescence imaging using dehydroergosterol as a fluorescent cholesterol analog. Biophys. J. *75*, 1915–1925.

Murphy, S.E., and Levine, T.P. (2016). VAP, a versatile access point for the endoplasmic reticulum: review and analysis of FFAT-like motifs in the VAPome. Biochim. Biophys. Acta *1861*, 952–961.

Olkkonen, V.M. (2015). OSBP-Related protein family in lipid transport over membrane contact sites. Lipid Insights *8*, 1–9.

Olkkonen, V.M., and Levine, T.P. (2004). Oxysterol binding proteins: in more than one place at one time? Biochem. Cell Biol. *82*, 87–98.

Otwinowski, Z., and Minor, W. (1997). Processing of X-ray diffraction data collected in oscillation mode. Methods Enzymol. *276*, 307–326.

Phillips, M.J., and Voeltz, G.K. (2016). Structure and function of ER membrane contact sites with other organelles. Nat. Rev. Mol. Cell Biol. *17*, 69–82.

Prinz, W.A. (2010). Lipid trafficking sans vesicles: where, why, how? Cell *143*, 870–874.

Raychaudhuri, S., and Prinz, W.A. (2010). The diverse functions of oxysterol-binding proteins. Annu. Rev. Cell Dev. Biol. *26*, 157–177.

Roberts, P., Moshitch-Moshkovitz, S., Kvam, E., O'Toole, E., Winey, M., and Goldfarb, D.S. (2003). Piecemeal microautophagy of nucleus in *Saccharomyces cerevisiae*. Mol. Biol. Cell *14*, 129–141.

Rocha, N., Kuijl, C., van der Kant, R., Janssen, L., Houben, D., Janssen, H., Zwart, W., and Neefjes, J. (2009). Cholesterol sensor ORP1L contacts the ER protein VAP to control Rab7-RILP-p150 Glued and late endosome positioning. J. Cell Biol. *185*, 1209–1225.

Roy, A., and Levine, T.P. (2004). Multiple pools of phosphatidylinositol 4-phosphate detected using the pleckstrin homology domain of Osh2p. J. Biol. Chem. *279*, 44683–44689.

Schulz, T.A., Choi, M.G., Raychaudhuri, S., Mears, J.A., Ghirlando, R., Hinshaw, J.E., and Prinz, W.A. (2009). Lipid-regulated sterol transfer between closely apposed membranes by oxysterol-binding protein homologues. J. Cell Biol. *187*, 889–903.

Tong, J., Yang, H., Yang, H., Eom, S.H., and Im, Y.J. (2013). Structure of Osh3 reveals a conserved mode of phosphoinositide binding in oxysterol-binding proteins. Structure *21*, 1203–1213.

Tong, J., Manik, M.K., Yang, H., and Im, Y.J. (2016). Structural insights into nonvesicular lipid transport by the oxysterol binding protein homologue family. Biochim. Biophys. Acta *1861*, 928–939.

van der Kant, R., Fish, A., Janssen, L., Janssen, H., Krom, S., Ho, N., Brummelkamp, T., Carette, J., Rocha, N., and Neefjes, J. (2013). Late endosomal transport and tethering are coupled processes controlled by RILP and the cholesterol sensor ORP1L. J. Cell Sci. *126*, 3462–3474.

Yang, H., Tong, J., Lee, C.W., Ha, S., Eom, S.H., and Im, Y.J. (2015). Structural mechanism of ergosterol regulation by fungal sterol transcription factor Upc2. Nat. Commun. *6*, 6129.

Zinser, E., and Daum, G. (1995). Isolation and biochemical characterization of organelles from the yeast, *Saccharomyces cerevisiae*. Yeast *11*, 493–536.

Zinser, E., Paltauf, F., and Daum, G. (1993). Sterol composition of yeast organelle membranes and subcellular distribution of enzymes involved in sterol metabolism. J. Bacteriol. *175*, 2853–2858.

STAR★METHODS

KEY RESOURCES TABLE

REAGENT or RESOURCE	SOURCE	IDENTIFIER
Bacterial and Virus Strains		
E. coli strain BL21(DE3)	New England BioLabs	Cat#C2527I
Chemicals, Peptides, and Recombinant Proteins		
Cholesterol	Sigma-Aldrich	Cat#C8503
Ergosterol	Sigma-Aldrich	Cat#45480
PI(4)P diC8	Avanti Polar Lipids	Cat#850182
Dihydroergosterol (DHE)	Sigma-Aldrich	Cat#E2634
DOPC (1,2-dioleoyl-*sn*-glycero-3-phosphocholine)	Avanti Polar Lipids	Cat#850375
DOPS (1-palmitoyl-2-oleoyl-*sn*-glycero-3-phospho-l-serine)	Avanti Polar Lipids	Cat#840035
Kluyveromyces lactis genomic DNA	ATCC	Cat#8585D-5
L-Selenomethionine	Tokyo Chemical Industry	Cat#S0442
Deposited Data		
KlOsh1 ANK apo structure	This paper	PDB: 5H2A
ScOsh1 ANK apo structure	This paper	PDB: 5H28
ScOsh1 ANK – Nvj1 fusion structure	This paper	PDB: 5H2C
KlOsh1 ORD – ergosterol complex structure	This paper	PDB: 5H2D
KlOsh1 ORD – cholesterol complex structure	This paper	PDB: 5WVR
Oligonucleotides		
Primer: ScOsh1 ANK Forward: GTATCTGGATCCTCGTCTGTGGCCATCAGTAAG	This paper	N/A
Primer: ScOsh1 ANK Reverse: GTATAATCTCGAGTCATGTGACGTCG	This paper	N/A
Primer: KlOsh1 ANK Forward: GTATTAGGATCCACTGTCTCAGTTTCGAAGCC	This paper	N/A
Primer: KlOsh1 ANK Reverse: GATACACTCGAGTCAATTGGTCACGTCTATAACAC	This paper	N/A
Primer: KlOsh1 ORD Forward: GTATAAGGATCCACAGCGGAACAGAAGACGAAAG	This paper	N/A
Primer: KlOsh1 ORD Reverse: GATACACTCGAGCTA AAAAATATCTCCTTCATCAG	This paper	N/A
Recombinant DNA		
pHIS2-KlOsh1 ANK	This paper	N/A
pHIS2-ScOsh1 ANK	This paper	N/A
pHIS2-ScOsh1 ANK-Nvj1	This paper	N/A
pHIS2-T4L-Nvj1 (residue 114-156)	This paper	N/A
pHIS2-KlOsh1 ORD	This paper	N/A
Software and Algorithms		
COOT	(Emsley et al., 2010)	http://www2.mrc-lmb.cam.ac.uk/personal/pemsley/coot
HKL2000	(Otwinowski and Minor, 1997)	http://www.hkl-xray.com/
Phenix	(Adams et al., 2010)	https://www.phenix-online.org

CONTACT FOR REAGENT AND RESOURCE SHARING

Further information and requests for reagents should be directed to and will be fulfilled by the Lead Contact, Young Jun Im (imyoungjun@jnu.ac.kr).

METHOD DETAILS

Cloning of Yeast Osh1 ANK and ORD Domains

The DNA, encoding the ANK domains of KlOsh1 (UniProt ID: Q6CUK7, residues 10-274) and ScOsh1 (UniProt ID: P35845, residues 7-274), was amplified by polymerase chain reaction (PCR) using the yeast genomic DNA as a template. The PCR products were subcloned into the BamHI/XhoI site of a modified pHIS-2 vector. The Osh1 ANK domains were tagged with an N-terminal hexahistidine, followed by a thrombin protease cleavage site (LVPR/GS). The DNA encoding the OSBP-related domain (ORD, residues 808-1240) of KlOsh1 was amplified by PCR using *Kluyveromyces lactis* genomic DNA as a template. The PCR product was subcloned into the BamHI/XhoI site of a modified pHIS-2 vector. The sequence alignment of the ORD domains suggested that the KlOsh1 ORD contains a long loop insertion between β15 and β16 compared to other Osh homologs. To improve the crystal quality of KlOsh1 ORD, three residues 1109-1111 in the flexible β15-β16 loop were deleted by PCR-based mutagenesis, and the loop-truncated ORD was used for structure determination.

Construction of Osh1 ANK–Nvj1 Chimera

To improve the crystallization properties of the ScOsh1 ANK–Nvj1 peptide complex, the Nvj1 segment (residues 139-165) was fused at the C-terminus of the ScOsh1 ANK. First, the DNA for the Nvj1 segment was amplified by PCR, to contain a 5' overhang of 15 nucleotides encoding the C-terminal sequence of Osh1 ANK. The Nvj1 PCR products and the forward primer of the Osh1 ANK were used as primers for the second round of PCR to amplify the DNA of the Osh1 ANK-Nvj1 fusion using Osh1 ANK as a template. The PCR product of the Osh1-Nvj1 fusion was subcloned into the BamHI/XhoI site of the pHIS-2 vector. The optimal length of the Nvj1 segment was determined empirically by testing the protein solubility and homogeneity of various Osh1 ANK-Nvj1 constructs.

Protein Expression and Purification

Escherichia coli strain BL21(DE3) cells, transformed with the plasm ids encoding the Osh1 ANK domains were grown to an OD600 of 0.8 at 310 K in the Luria-Bertani medium. Cells were induced by adding isopropyl β-D-1-thiogalactopyranoside to a final concentration of 0.25 mM, and were incubated for 12 h overnight at 293 K prior to harvesting. Cells expressing the Osh1 ANK were resuspended in 2X phosphate buffered saline (PBS) containing 20 mM imidazole and lysed by sonication. The supernatant containing the His-Osh1 ANK was applied onto a Ni-NTA affinity column. The Ni-NTA column was thoroughly washed with the lysis buffer. The fusion protein was eluted from the column using 100 mM Tris-HCl pH 7.5, 300 mM imidazole, 300 mM NaCl. The eluate was concentrated to 10 mg/ml, and the His-tag was removed by cleavage with thrombin protease. The Osh1 ANK protein was subjected to size exclusion chromatography using a Superdex 200 column (GE healthcare) equilibrated with 20 mM Tris-HCl pH 8.0, 150 mM NaCl. The peak fractions containing the Osh1 protein was concentrated to 10 mg/ml for crystallization. The selenomethionyl protein for the KlOsh1 ANK was expressed in a heterotrophic *E. coli* strain BL21(DE3) by a methionine pathway inhibition technique (Doublie, 1997) and the protein was purified by the same procedure as that used for the native protein described above.

The Osh1 ORD was tagged with an N-terminal hexahistidine followed by a thrombin protease cleavage site (LVPR/GS). *Escherichia coli* strain BL21(DE3) cells containing Osh1 ORD plasmids were grown to an OD600 of 0.8 at 310 K in the LB medium. To facilitate protein folding of the ORD domain by providing a sterol ligand, 20 mg of ergosterol, or cholesterol, was added per 1L culture during protein expression. Cells were induced by the addition of isopropyl β-D-1-thiogalactopyranoside to a final concentration of 2.5 mM and were incubated for 12 h overnight at 293 K prior to harvesting. The Osh1 ORD was purified by the same procedures as those used for the purification of Osh1 ANK. In addition, 10 mg of ergosterol, or cholesterol, was added during cell lysis to saturate the sterol-binding sites with the ligands.

Crystallization and Crystallographic Analysis

The preliminary crystallization experiments for the ANK and ORD domains of KlOsh1 and ScOsh1 were carried out at 295 K in 96-well crystallization plates using a multichannel pipette and customized crystallization-screening solutions by dispensing 0.8 μl protein solution and 0.8 μl precipitant solution. The initial crystals of ScOsh1 ANK appeared after 5 days in a solution consisting of 0.1 M HEPES-NaOH pH 7.0, 20% PEG 1500. The crystallization condition was further optimized using the hanging-drop technique in 15-well screw-cap plates. A drop consisting of 2 μl protein solution was mixed with 2 μl precipitant solution and equilibrated against 1 ml reservoir solution. High-quality crystals with dimensions of 0.1 × 0.1 × 0.15 mm, appeared in 1 week.

The crystals of the KlOsh1 ANK were grown using a solution consisting of Bicine-HCl pH 9.0, 20% PEG 3350, 0.2 M $MgSO_4$. Streak seeding techniques were used to improve crystal size and quality suitable for the x-ray diffraction experiments. The KlOsh1 ORD was crystallized using a solution consisting of 0.1 M citrate-NaOH pH 4.0, 25% PEG 8000, 0.2 M Li_2SO_4. Crystals of the Osh1 ANK and ORD were cryoprotected in a reservoir solution supplemented with 10% glycerol, and flash-cooled by immersion in liquid nitrogen. Crystals were preserved in a cryogenic N_2-gas stream (~100 K) during the diffraction experiments. Diffraction data for the native Osh1 ANK were collected at a fixed wavelength of 0.97949 Å using an ADSC Q270 CCD detector on the 7A and 5C beamlines at Pohang Light Source (PLS), Pohang Accelerator Laboratory, Republic of Korea. All data were processed and scaled using HKL-2000 (Otwinowski and Minor, 1997) and handled with the CCP4 program suite. The structure of the KlOsh1 ANK was determined by using single anomalous dispersion (SAD) method using selenomethionyl KlOsh1 crystals. The diffraction data were collected at a wavelength of 0.97934 Å to 2.8 Å resolution and SAD phasing was done using the software Phenix (Adams et al., 2010). Two molecules of KlOsh1 ANK were clearly visible, and a preliminary model was build using the program Coot (Emsley et al., 2010).

Subsequently, the initial model was transferred to the native data set with 1.9 Å resolution and the final model was refined to R_{work}/R_{free} values of 18.8%/22.2%. The structures of KlOsh1 ORD were determined by molecular replacement using the structure of yeast Osh3 ORD (PDB code: 4INQ) as a search model. Density modification showed clear electron densities of the Osh1 ORD and the bound ergosterol or cholesterol. The 15 residues at 1048-1051 in the β12-β13 loop, and at 1096-1107 in the β15-β16 loop, were not visible due to disorder and were not modeled. The final models of the Osh1 ORD in complex with ergosterol or cholesterol were refined to R_{work}/R_{free} values of 17.7%/21.0% and 19.1%/22.3%, respectively.

Isothermal Titration Calorimetry of the Osh1 ANK-Nvj1 Interaction

The DNA for the ScNvj1 segment (residues 114-156) was cloned into the pHis-T4L vector providing the N-terminal cleavable His-tag and T4 lysozyme fusion. The T4L-Nvj1 was purified by the same procedure used for the Osh1 ANK. The binding experiments of Osh1 and Osh2 ANKs with Nvj1 were performed using a VP-ITC calorimeter (V_{cell} = 1.40 ml; MicroCal, Northampton, MA) at 20°C. All proteins were dissolved in a buffer containing 20 mM Tris-HCl pH 7.5, 150 mM NaCl. Then, 2.4 mM of ScOsh1 ANK, or 1.5 mM of KlOsh1 ANK, was loaded into the syringe, and 0.4 mM of T4L-ScNvj1 was placed in the cell. The titration curve was obtained by injecting 11-μl aliquots of Osh1 ANK proteins into the cell containing T4L-ScNvj1, at a time interval of 300s. The enthalpy of reaction, ΔH^0, the binding constant, K, and the stoichiometry value, n, were calculated from the measured heat changes, δH_i, upon the association of Osh1 ANK and T4L-Nvj1. The titration data were analyzed using the program Origin 7.0 and fitted by the one-site binding model.

Preparation of the Liposomes

DOPC (1,2-dioleoyl-*sn*-glycero-3-phosphocholine) and POPS (1-palmitoyl-2- oleoyl-*sn*-glycero-3-phospho-l-serine) were obtained from Avanti Polar Lipids Inc. Ergosterol and DHE were obtained from Sigma-Aldrich. The DOPC/ergosterol liposomes were prepared as described previously with slight modifications (Yang et al., 2015). The lipids were dissolved in chloroform or ethanol, mixed at the desired molar ratio, incubated at 37°C for 5 min, and then the solvent was evaporated using a stream of nitrogen gas. The dried lipids were resuspended in 50 mM HEPES-NaOH pH 7.2, 120 mM potassium acetate by vortexing. The liposomes were prepared at a total lipid concentration of 1.0 mg/ml. The hydrated lipid mixture was frozen and thawed five times using a water bath and ethanol at -70°C. The lipid mixture was extruded 10 times through a polycarbonate filter with a pore size of 0.1 mm. The liposomes were stored at 4°C and used within 24 h.

Sterol and PI(4)P Binding Assays Using FRET

Fluorescent measurements of sterol binding to the KlOsh1 ORD were based on FRET between the Trp and bound DHE, and were conducted using a method reported previously with a slight modification (Yang et al., 2015). Trp fluorescence was measured at 340 nm (with a bandwidth of 5 nm) with an excitation at 285 nm using a spectrofluorometer (FP-6200; JASCO). Emission spectra were recorded at several time points to monitor the changes of ligand binding. The recombinant KlOsh1 ORD was purified as an ergosterol complex. We could not purify the homogeneous KlOsh1 ORD in its apo-form because of the protein aggregation. For the DHE binding assay, 1 μM of the purified KlOsh1 ORD was incubated with 2.5 μM of DHE for 14 h at 4°C. This allows replacement of ergosterol with DHE by competitive binding to the KlOsh1 ORD. The binding of DHE was confirmed by monitoring the change in the fluorescence spectrum of the mixture when the tryptophan residues of KlOsh1 ORD were excited at 285 nm. Tryptophan quenching at 340 nm, caused by the DHE binding, was accompanied by the appearance of three emission peaks at 354, 373, and 393 nm. The addition of DOPC:ergosterol (at the molar ratio of 2.3:1) liposomes to the DHE-loaded KlOsh1 at a final concentration of 50 μg/μl eliminated the unique DHE fluorescence. This suggests that the KlOsh1 ORD exchanged the DHE for the ergosterol uptaken from the liposomes. To examine the PI(4)P/sterol exchange properties of the Osh1 ORD, the fluorescence spectrum was monitored upon the addition of 3.2 μM soluble PI(4)P diC8 to the DHE-loaded Osh1 ORD. The disappearance of unique DHE spectrum upon the PI(4)P addition suggests that PI(4)P replaced the sterol in the ligand-binding pocket of the Osh1 ORD.

Structure, Volume *25*

Supplemental Information

Structure of Yeast OSBP-Related Protein Osh1 Reveals Key Determinants for Lipid Transport and Protein Targeting at the Nucleus-Vacuole Junction

Mohammad Kawsar Manik, Huiseon Yang, Junsen Tong, and Young Jun Im

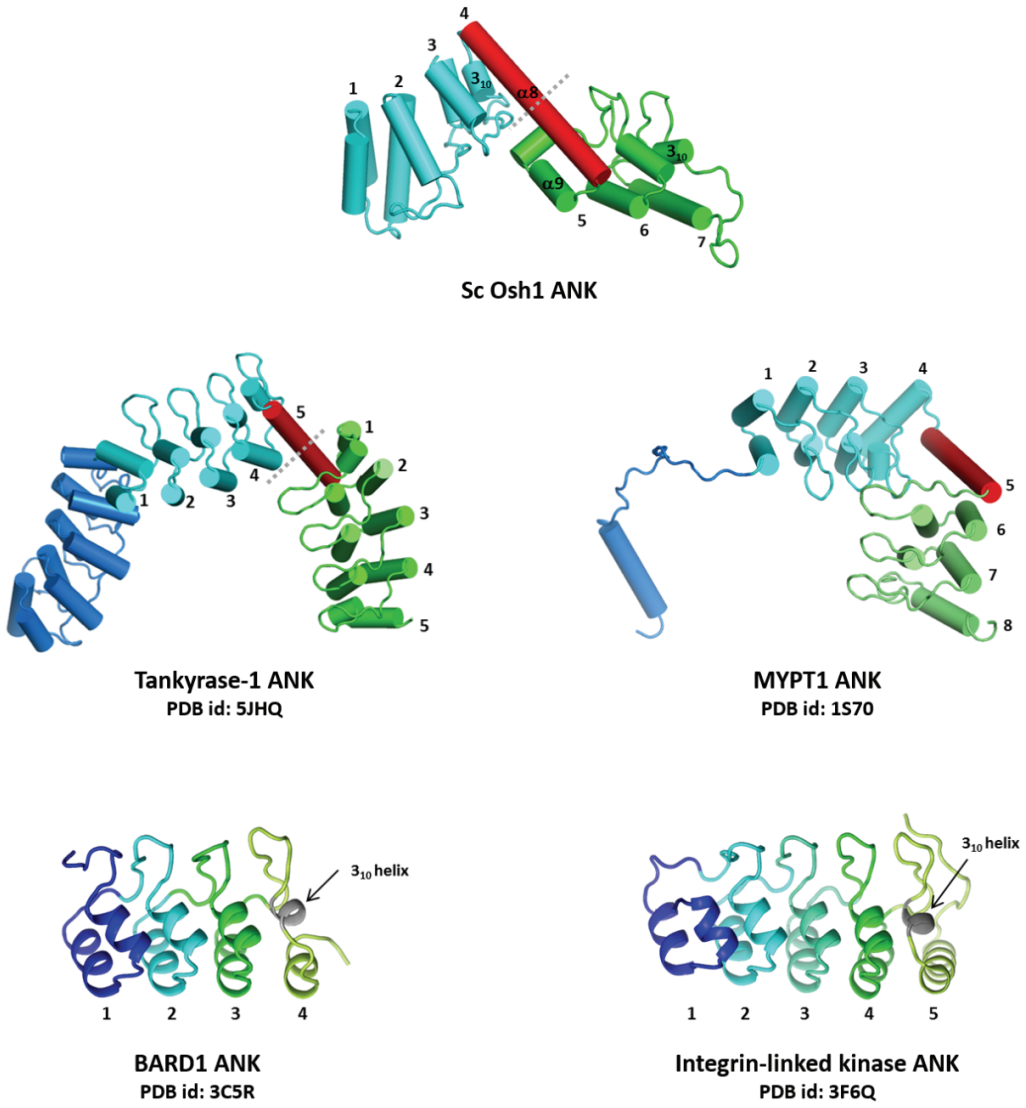

Figure S1, related to Figure 1. Structural similarity of the Osh1 ANK to other ANK domain. The structurally related ANK domains found by DALI similarity search, Tankyrase-1 ANK (PDB id 5JHQ) (Eisemann et al., 2016) and Myosin phosphatase targeting subunit MYPT1 ANK (PDB id 1S70) (Terrak et al., 2004), are shown in cylindrical representation. The assignment of ANK repeats for Tankyrase-1 was based on the report (Guettler et al., 2011). The subdomains in one polypeptide are colored blue to green from the N- to C-terminus. The connecting α-helix is shown in red. The numbers indicate consecutive ankyrin repeats. Two ANK domains containing a 3_{10} helix in the terminal repeat are shown in ribbon representation.

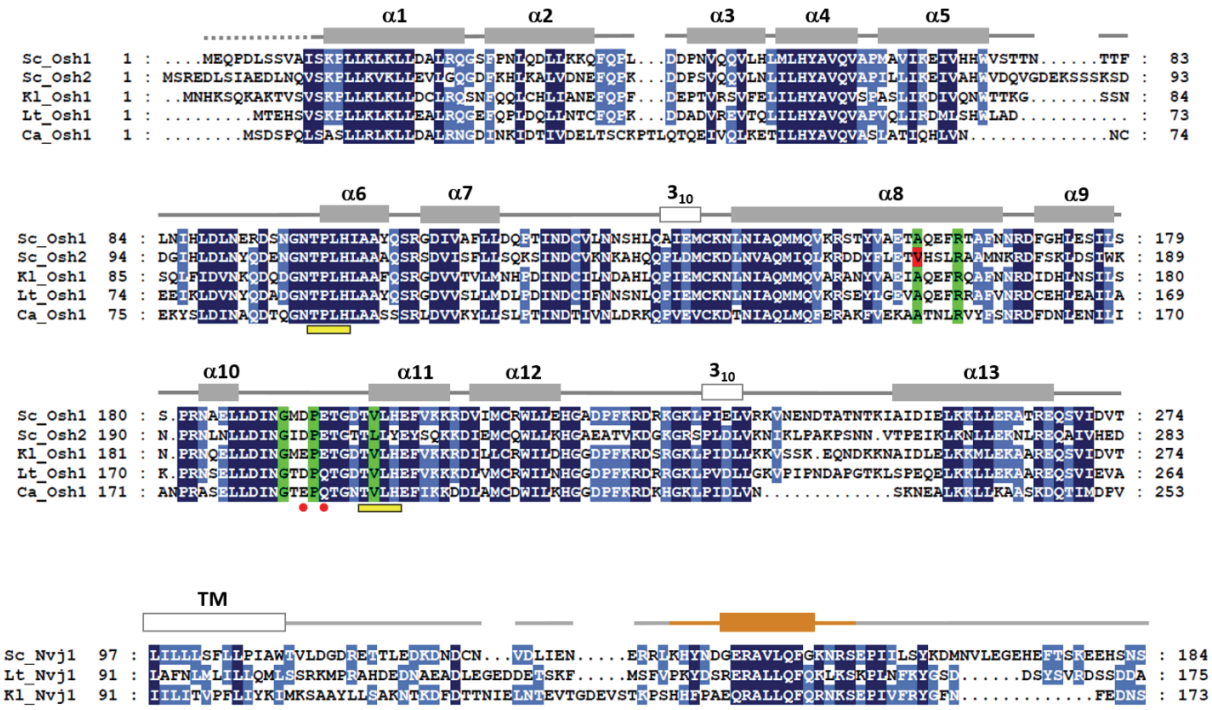

Figure S2, related to Figure 1 and 3. Sequence alignments of Osh1 ANK domains and Nvj1 segments from the yeast species.

The top two sequences of the ANK domains are from Osh1 and Osh2 of *Saccharomyces cerevisiae*; Osh1 orthologs from other species are shown with abbreviations as follows: *K.l.* (*Kluyveromyces lactis*); *C.a.* (*Candida albicans*); *L.t.* (*Lachancea thermotolerans*). Conserved residues are colored in dark blue and light blue, depending on their respective degree of conservation from highest to lowest. The key residues directly interacting with Nvj1 segment are shaded in green. The variable residue Val169, in Osh2, which interferes with the Nvj1 binding is shaded in red. Glu195 and Asp193 of Osh1, forming salt bridges with His140 and Arg146 of Nvj1, are indicated by the red spheres. The bottom panel shows a sequence alignment of Nvj1 segments from fungal homologs. The open square indicates the nuclear transmembrane region of Nvj1. The binding site for the Osh1 ANK in Nvj1 is colored in orange. The conserved TPLH tetrapeptide motif in the ANK repeats are indicated by yellow rectangles.

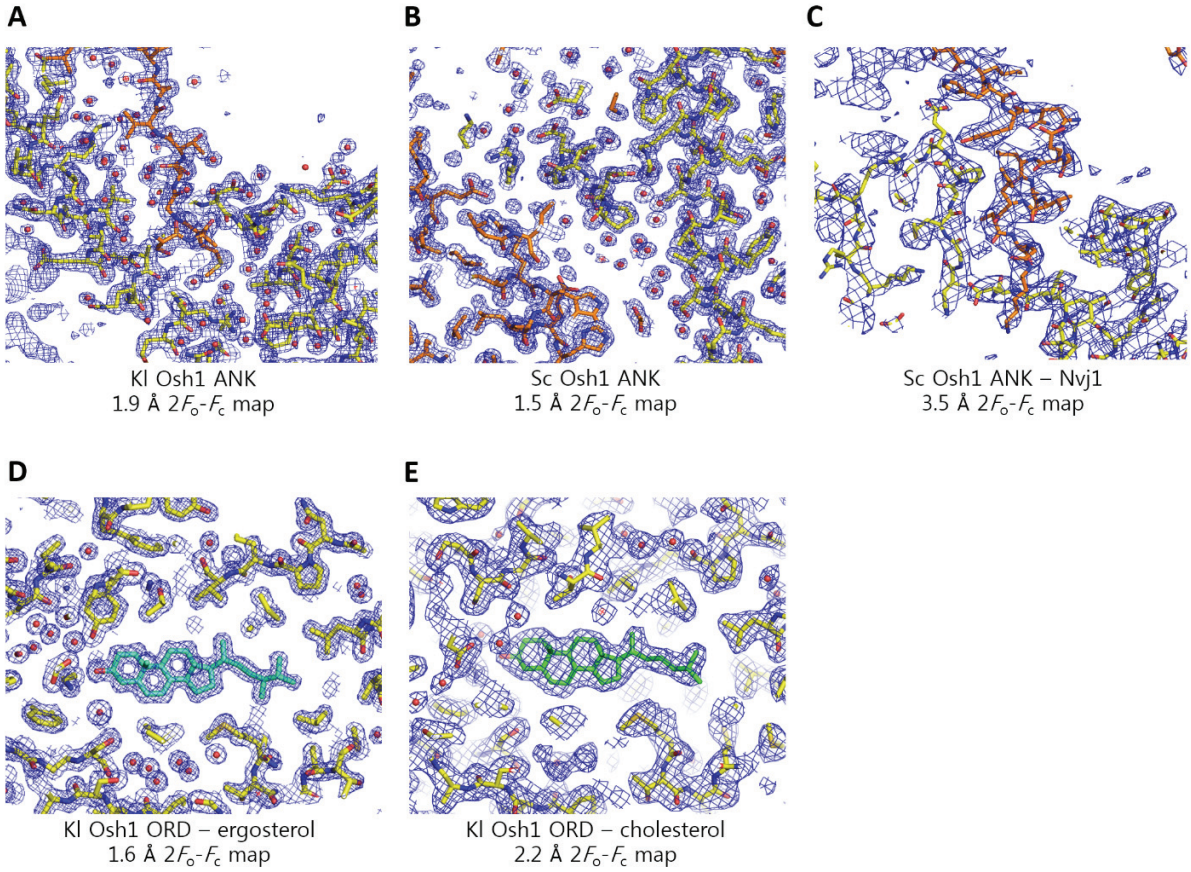

Figure S3, related to Figure 1, 3, and 6. Electron density maps

(A) The 1.9 Å 2*Fo*-*Fc* map of apo KlOsh1 ANK with the final model superimposed.

(B) The 1.5 Å 2*Fo*-*Fc* map of apo ScOsh1 ANK with the final model superimposed.

(C) The 3.5 Å 2*Fo*-*Fc* map of ScOsh1 ANK-Nvj1 fusion with the final model superimposed. The orange sticks represent the Nvj1 segment and the yellow represent Osh1 ANK.

(D) The 1.6 Å 2*Fo*-*Fc* map of KlOsh1 ORD-ergosterol complex with the final model superimposed.

(E) The 2.2 Å 2*Fo*-*Fc* map of KlOsh1 ORD-cholesterol complex with the final model superimposed.

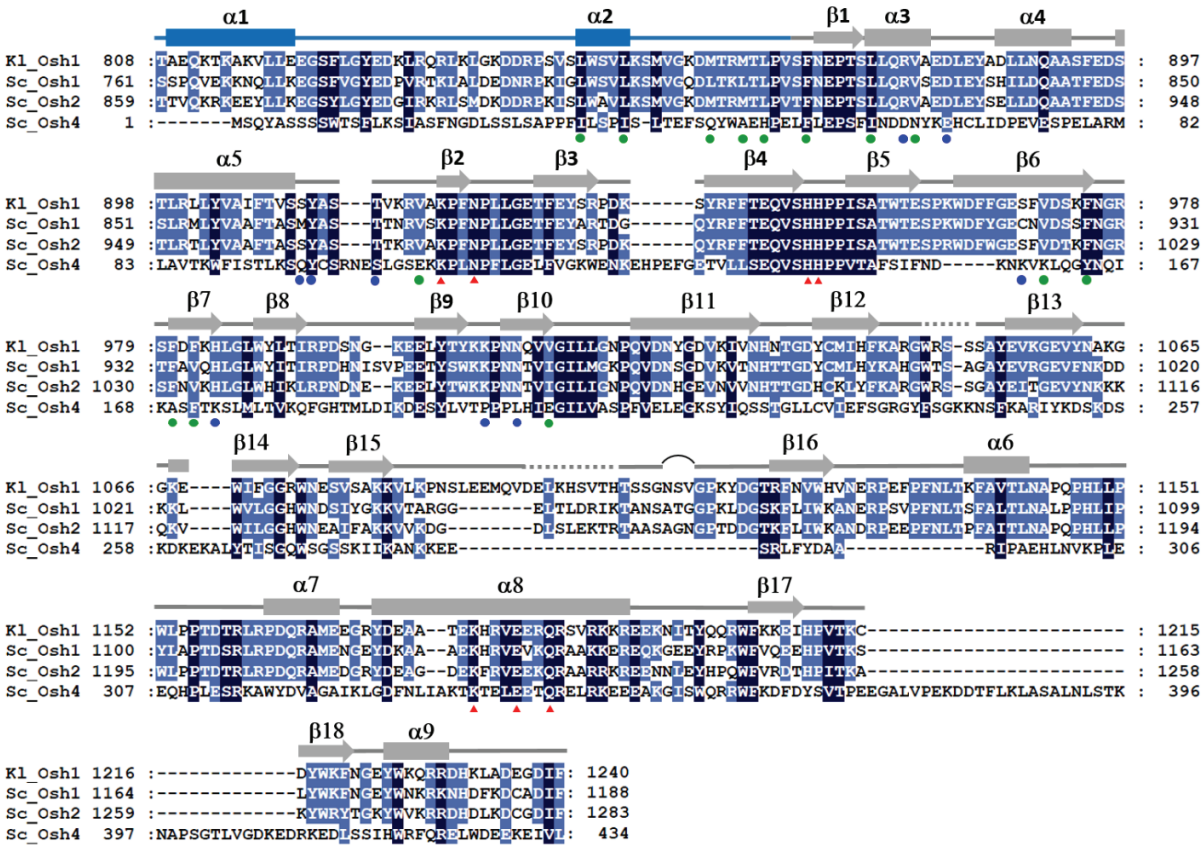

Figure S4, related to Figure 5 and 6. Sequence alignments of ORD domains from the yeast Osh1 homologs

Amino acid sequence alignments of ORDs from yeast ORPs. Sequences were initially aligned using the program ClustalX and were manually rearranged for the C-terminal regions with low sequence conservation based on the structural superposition of Osh1 and Osh4. The conserved residues in the ORD, recognizing the head group of the PI(4)P ligand, are indicated as red triangles. The residues on the wall of the hydrophobic tunnel are shown as green dots. Polar residues at the bottom of the tunnel are indicated as blue dots. The KlOsh1 ORD construct used for structure determination contains three residue deletions in the β15-β16 loop, which is indicated by a convex line between the residue 1109 and 1111. The disordered residues not modeled in the structure were indicated by the dotted lines.

Refrences

Eisemann, T., McCauley, M., Langelier, M.F., Gupta, K., Roy, S., Van Duyne, G.D., and Pascal, J.M. (2016). Tankyrase-1 Ankyrin Repeats Form an Adaptable Binding Platform for Targets of ADP-Ribose Modification. Structure *24*, 1679-1692.

Guettler, S., LaRose, J., Petsalaki, E., Gish, G., Scotter, A., Pawson, T., Rottapel, R., and Sicheri, F. (2011). Structural basis and sequence rules for substrate recognition by Tankyrase explain the basis for cherubism disease. Cell *147*, 1340-1354.

Terrak, M., Kerff, F., Langsetmo, K., Tao, T., and Dominguez, R. (2004). Structural basis of protein phosphatase 1 regulation. Nature *429*, 780-784.